Contents lists available at ScienceDirect

Journal of Petroleum Science and Engineering

journal homepage: http://ees.elsevier.com

Building a rock physics model for the formation evaluation of the Lower Goru sand reservoir of the Southern Indus Basin in Pakistan

Muhammad Ali [a], Huolin Ma [a,*], Heping Pan [a], Umar Ashraf [b], Ren Jiang [c]

[a] Institute of Geophysics & Geomatics, China University of Geosciences, Wuhan, Hubei, 430074, PR China
[b] College of Ecology and Environment Sciences, Yunnan University (Chenggong Campus), Kunming, Yunnan, 650500, PR China
[c] Research Institute of Petroleum Exploration and Development, Petrochina Company Limited, Beijing, PR China

ARTICLE INFO

Keywords
Lower goru sand reservoir
Rock physics model
Rock physics template
Well logs
Petrophysical analysis

ABSTRACT

The geological factors of any reservoir, such as porosity, lithology, and fluid characteristics, control the rock physics models. Several retrospective studies have discussed the methods of discriminating and calculating these geological factors in the Lower Goru sand reservoir. Therefore, it is imperative to build the best-modified suitable rock physics model and template to diagnose an inadequately consolidated reservoir that has been previously overlooked. For the purpose, the research evaluates a dataset of five wells to develop a modified rock physics model and template for a Lower Goru sand reservoir in Pakistan. The study compares and evaluates different rock physic models such as Stiff sand, Friable-sand, Greenberg and Castagna, and Raymer's model to calibrate the best model, which would comprehensively assist the future researchers. According to the results, Stiff sand is quite a suitable rock physics model. Furthermore, the rock physics template (RPT) is utilized to test the reliability of the predicted model that is helpful for the formation evaluation, reservoir characterization, and prospect evaluation across different fields of the Lower Goru sand reservoir. The predicted model can be further used to estimate porosity from the seismically derived impedance in the entire Lower Goru sand reservoir, Pakistan, and worldwide which has the same geological trends and reservoir distribution.

1. Introduction

A rock physics model is an essential tool for an effective interpretation of reservoir rock because it provides a vital link between reservoir properties and petrophysical paramters (Avseth, 2000; Chi and Han, 2009; He et al., 2011; Khalid et al., 2014). Usually, the petrophysical analysis is used to calculate and discriminate the properties such as shale content, sorting, porosity, lithology, and fluid characteristics (Castagna and Swan, 1997; Ahmed et al., 2016; Chi and Han, 2009; He et al., 2011). Avseth et al. (2005) has comprehensively categorized various inclusions models (Berryman and Laboratories, 1980; Cheng and Toksöz, 1979; Kuster and Toksöz, 1974; Liu and Sun, 2015), contact models (Dvorkin et al., 1994; Dvorkin and Nur, 1996; Mindlin, 1949; Walton, 1987), transformations (Berryman and Milton, 1991; Gassmann, 1951), bounds (Hashin and Shtrikman, 1963; Hill, 1952; Reuss, 1929; Voigt, 1910) and computational models. A recent study by Azeem et al. (2017) focused on the discriminating reservoir and non-reservoir characterization, while others have focused on understanding the seismic parameters like compressional and shear wave velocities, elastic moduli, and density in Lower Goru sand reservoir (Zahid et al., 2016).

Rock physics modeling and petrophysical interpretation of wireline log data provide an outline for the evaluation of seismic elastic rock properties (Gray et al., 2015; Mavko and Mukerji, 1998). Therefore, for modeling of rock physics and interpretation of geophysical log, the usage of the logs data is essential for the calibration of elastic logs. Subsequently, to cover a vertical interval of interest between density, compressional sonic, and often shear sonic logs seem to be consistent. Thus, it is quite hard to satisfy the criteria of good quality log data due to various reasons; there are variations in tool measurements, environments, fluids and formations of the borehole, and poorness in the quality of logging situations that is conditioned with correction and synthesizing the log data for a complete and reliable characterization of reservoir study. The corollary, it is also vital to manage missing data to accomplish the elastic logs of the wells and Zone of Interest (ZOI).

In the recent years, multiple studies have been conducted on the petrophysical analysis to estimate the reservoir potential of the Lower Goru sand reservoir, Pakistan (Ali et al., 2019; Ashraf et al., 2019a, 2019b; Hussain et al., 2017; Ismail et al., 2017; Khan and

* Corresponding author.
E-mail address: mhl70@163.com (H. Ma)

https://doi.org/10.1016/j.petrol.2020.107461
Received 15 March 2020; Received in revised form 14 April 2020; Accepted 27 May 2020
Available online xxx
0920-4105/

Khan, 2018; Khan et al., 2017; Yasin et al., 2019). Khalid et al. (2014) have come up with a modified RPD based on the thermodynamic properties of reservoir fluids at in situ conditions and Azeem et al. (2017) has adopted the Xu–White model to investigate the litho-fluid behavior, but were unable to provide a reliable rock physics model and template which will accurately provide the geology trend and reservoir behavior of the whole Lower Goru Formation. Yasin et al. (2017) described that it is quite contemporary and common to estimate the hydrocarbon potential from poor-quality reservoirs rock in Pakistan. Being an emerging economy, the exploration and development sector of oil and gas companies in Pakistan needs to understand the proper reservoir distribution and geology trend of these poor quality reservoirs for the economic appraisals (Ashraf et al., 2016). Therefore, to diagnose a poor-quality and consolidated reservoir, it is essential to build the best suitable rock physics model and template that has been previously neglected. Consequently, the research focuses on developing a reliable rock physics workflow for the building of a rock physics model for the Lower Goru Sand Reservoir, Pakistan.

For the interest, a dataset of five wells from Lower Goru sand was used in the current study. The study compares and evaluates different rock physic models such as Stiff sand (Mavko et al., 2009), Friable-sand (Dvorkin and Nur, 1996), Raymer's model(Raymer et al., 1980) and the Greenberg and Castagna (1992) to calibrate the best model which enables to study the reservoir behaviour. The study employs fluid substitution of Gassmann (1951) to estimate seismic velocity and pore impedance when the bulk module changes when pores are filled with various fluids. Based on rock physics scenarios, the model of fluid replacement is utilized to differentiate fluids like water saturation, porosity, and density of oil. Accordingly, the study aims to build a rock physic model from the existing geological information including petrophysical properties which will benefit petrophysicists, geologists and geophysicists across the Pakistan which are working on the Lower Goru sand reservoir.

2. Geology of the study area

The area of research (Sawan) is situated in the Southern Indus Basin, which is also mentioned as “Lower Indus Basin (LIB)” (Ashraf et al., 2019a, 2019b). Southern Indus Basin is situated in all the way that Indian Shield is situated in the West; Kirther Ranges and Thrust Belt, Sulaiman Fold in the East; in the south Khairpur-Jacobabad High and the North Sargodha High (Kazmi and Jan 1997; Afzal et al., 2009) (Fig. 1a). The research area is in the northwest direction, the Khairpur High is situated, which is characterized by a very high geothermal gradient related to present up to 4.8 °C/100 m (Azeem et al., 2016). Khairpur High plays a crucial role for the formation of traps are structural in the surrounding areas of the Miano field, Kadanwari field, Sawan gas field (Ahmad and Chaudhry, 2002; Ali et al., 2019; Ashraf et al., 2019a, 2019b; Berger et al., 2009). Because the Indus Basin (Upper, Central, and Lower) is rich in hydrocarbons and covers few complete petroleum systems, the numbers of wells in the Lower and Central Indus Basin were drilled. Organically rich, black-colored shales are deposited in a retired marine, oxygen-depleted environment, which is considered to be the best source rocks (Munir et al., 2011). In the area of research, the Sembar Formation of lower Cretaceous shale, is a proven source for hydrocarbon discovered in the area since of its organic richness and thermal maturity (Kazmi and Jan 1997). The Formation of Sembar is superimposed by the Goru Formation of Early Cretaceous age, which is separated into two different parts, Lower Goru Formation (LGF) and the Upper Goru Formation (UGF) (Kadri, 1995). The LGF comprises of shale, limestone, sandstone, and siltstone (Berger et al., 2009; Kazmi and Jan 1997). An upper part of the Lower Goru Formation has been dominated by mainly shale and limestone (Anwer et al., 2017). The lower portion of the LGF has been dominated by basal and massive sands (Ahmad et al., 2004). The Goru Formation was deposited in shoreface to the fluvial-based proximal delta-front depositional settings of the shallow marine environment (Ashraf et al., 2019a, 2019b; Khan et al., 1999). The fluvial-based depositional systems have very coarse to fine, porous and permeable sediments that are deposited in the fluvial channels and forms the reservoirs (Anees et al., 2019). The Lower Goru Formation also comprises of very coarse to fine sediments and form the main reservoir rock in the LIB (Qiang et al., 2020). The LGF can be categorized into four mian intervals A, B, C and D (Krois et al., 1998) (Fig. 1b). Where, D, B, and C intervals perform as a hydrocarbon reservoir potentially.

3. Materials and methodology

In the current research, the well-log data of five Sawan wells, namely Sawan well-01, Sawan well-02, Sawan well-03, Sawan well-07, and Sawan well-08, are employed to accomplish a novel rock

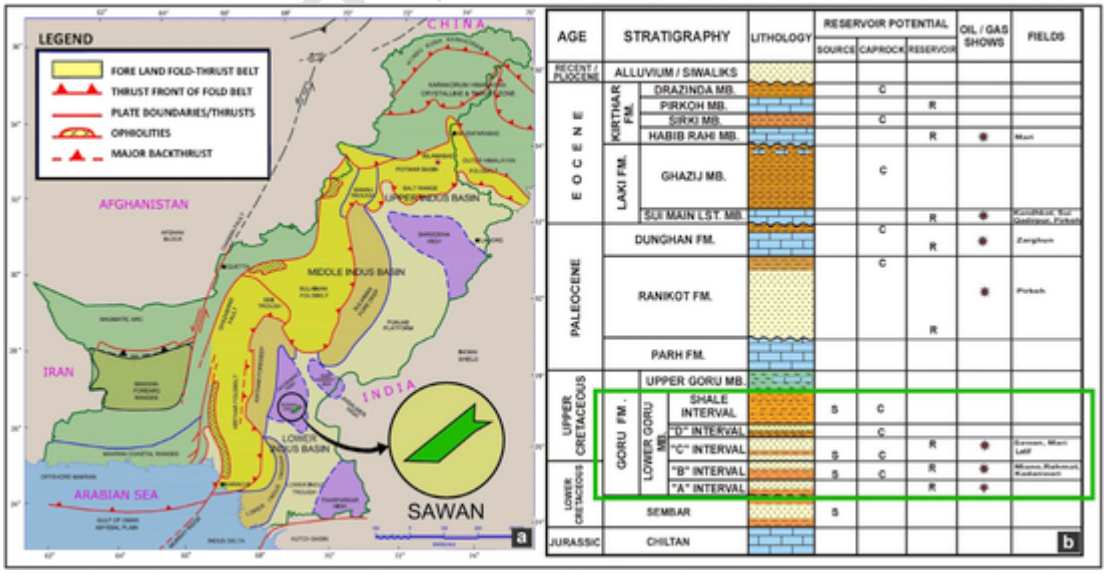

Fig. 1. (a) The map displaying the geology setting and significant sedimentary basins of Pakistan. The position of the study area is highlighted by a black arrow; (b) Generalized stratigraphy of the LIB. The green rectangle highlights the LGF. The C-sand interval is the main gas-producing reservoir of the area of study. (For interpretation of the references to color in this figure legend, the reader is referred to the Web version of this article.)

physics model and template for a heterogeneous sand-shale reservoir. The gamma-ray (GR), neutron porosity (NPHI), density (RHOB), P-sonic (DT), S-sonic (DTS), shallow resistivity (LLS), and deep resistivity (LLD) geophysical logs were evaluated to estimate the elastic logs which are employed to develop the rock physics model (RPM) and template (RPT) specifically for the LGF of the Lower Indus Basin, Pakistan.

To improve the log data's qualities and estimate the properties of the reservoir such as porosity, shale volume, and water saturation, the workflow of the methodology initially applies conditioning data and petrophysical analysis over the zone of interest (Fig. 2). In the second step, missing shear velocity is generated in the reservoir zone using Greenberg and Castagna techniques. Later, the elastic parameters are estimated. The third step determines the petrophysical parameters to calibrate the Gassmann Fluid Substitution model. Then, modeled and measured elastic parameters are log tracked to examine the matching degrees. Several diagnostic models of rock physics are compared and evaluated to describe a clastic reservoir's velocity-porosity behavior. Lastly, Local geology constrained the modeled response to create a modified rock physics model and template. Several methodologies are adopted to conduct this research which are as follows;

3.1. Data quality and well-log conditioning

In the study area, washout intervals are responsible for affecting the density and sonic logs. Therefore, the sonic waves are attenuated, which results in skipping the log curve. It occurs when the wave signal at the first arrival attenuates and at higher travel times shows a spike or an abrupt change (Rider, 2002). Diverse methods will remove cycle skips. Despite, filter is a first technique that used smooth median on flags of cycle skipping to remove values in range (Burch, 2002). The other technique describes a link among the additional well logs like gamma-ray (GR), resistivity (LLD), and density (RHOB), etc. against sonic slowness to come up with a model to interchange compressional data with cycle skip intervals. Both methods are used to eliminate unnecessary log spikes and to fill out the gap information of the logs that increases the log consistency in the study wells.

Generally, bulk density and compressional velocity (*Vp*) has a strong relationship (Gardner et al., 1974); thus, that when the density rises, velocity also rises. For brine-saturated sedimentary rocks, Gardner et al. (1974) developed a group of relations between compression velocity (*Vp*) and bulk density (Eq. (1)) using laboratory measurements.

$$\rho_{syn} = a * (V_p)^b \quad (1)$$

where *Vp* = compressional velocity (*m/s*), ρ_{syn} = density (g/cm^3), a = 0.31 when *Vp* is in *m/s* (b = 0.23), and *Vp* is in *ft/s* (b = 0.25).

The density tools are usually operated near the wall of borehole and are completely in touch with the borehole wall. So, environment of borehole harshly affects its logs like drilling fluid and tool position. Borehole irregularities influenced the density data in the Sawan well-03 well and the Gardner relationship is used in the focus region for generating the density curve. Moreover, in this analysis, the compressional velocity logs in a few depth intervals are de-spiked. In contrast, density logs are also harshly affected in the elliptical hole or washed-out interval. A multi-variable regression technique has been adopted to synthesize the log-curve in the washout intervals before these logs are subjected to processing. The log track in Fig. 3 confirms that the reliability of the synthetic density log. It displays a fine tie with the measured data over the decent borehole portion. Therefore, the density data can be substituted by the bad hole portion where invalid calculated data is present. The similar methods are utilized to condition measured sonic and density log curves for each well employed in this research, where the quality of the data was bad or gaps. Before conducting a petrophysical analysis, a necessary zone-wise consistency check is analyzed using the histograms of duo density and sonic logs of all the study wells together. Figs. 4 and 5 show the improvement of pattern in the histogram and crossplots of conditioned data as compared to raw ones for different formations.

3.2. Petrophysical parameters

3.2.1. Volume of shale

Gamma rays are necessary to determine the shale's presence in the formation evaluation workflow if any radioactive minerals are absent in rock formation (Rider, 2002). The index of gamma-ray ($Index_{GR}$) can be defined as (Eq. (2)).

$$Index_{GR} = \frac{GR_{log} - GR_{min}}{GR_{max} - GR_{min}} \quad (2)$$

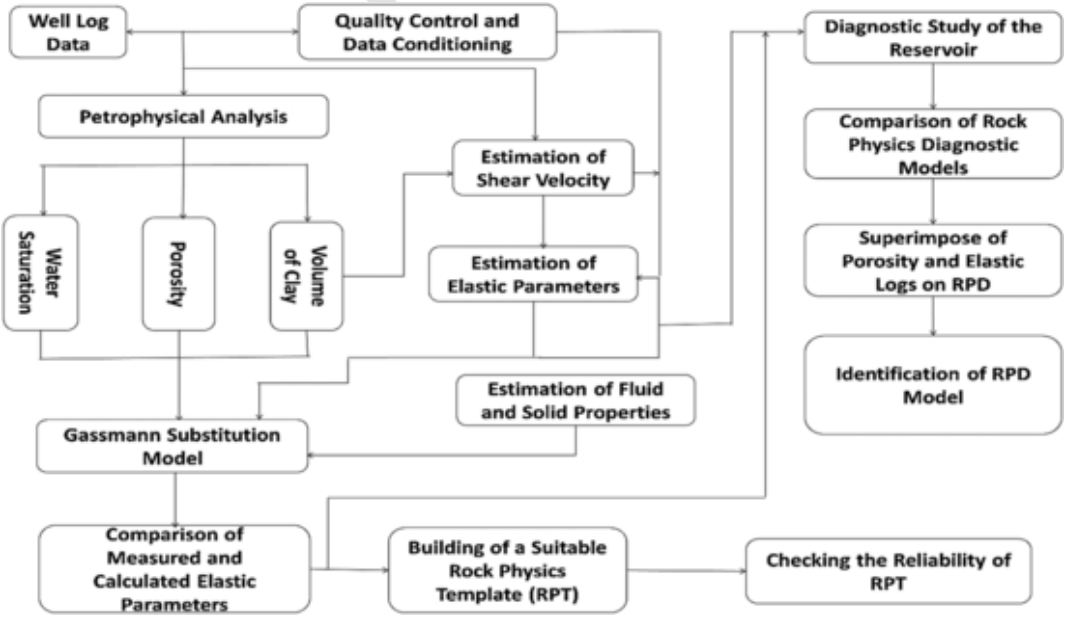

Fig. 2. Integrated workflow of petrophysics and rock-physics for the development of a rock physics model.

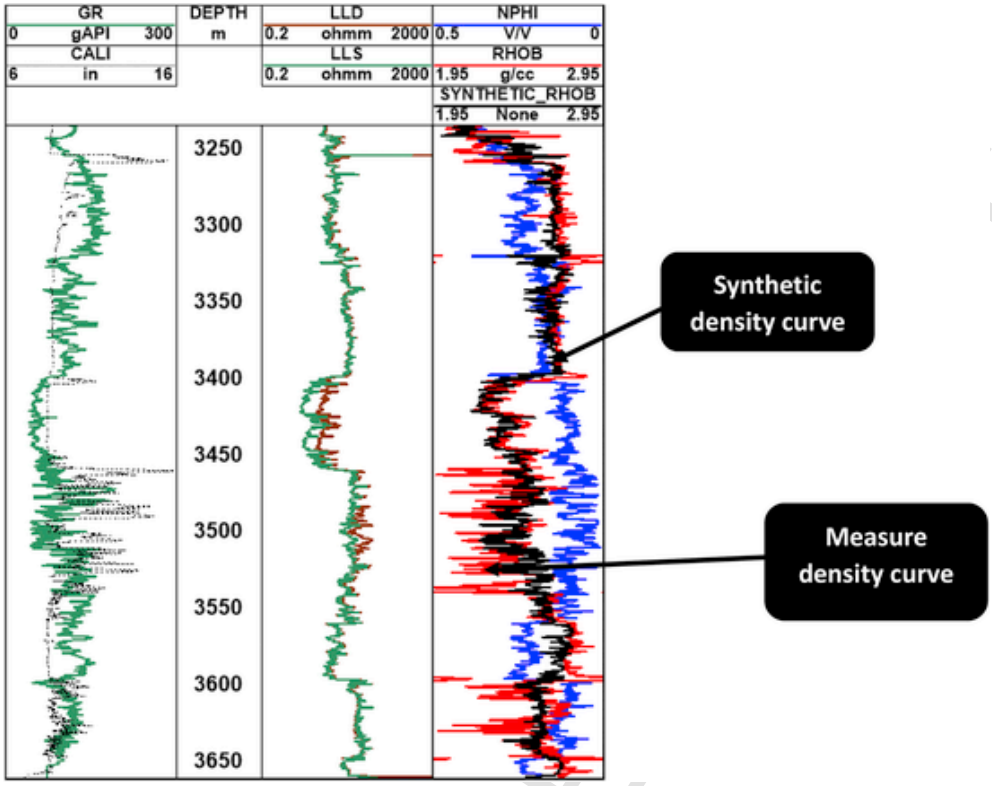

Fig. 3. Log condition and synthetic curve generation.

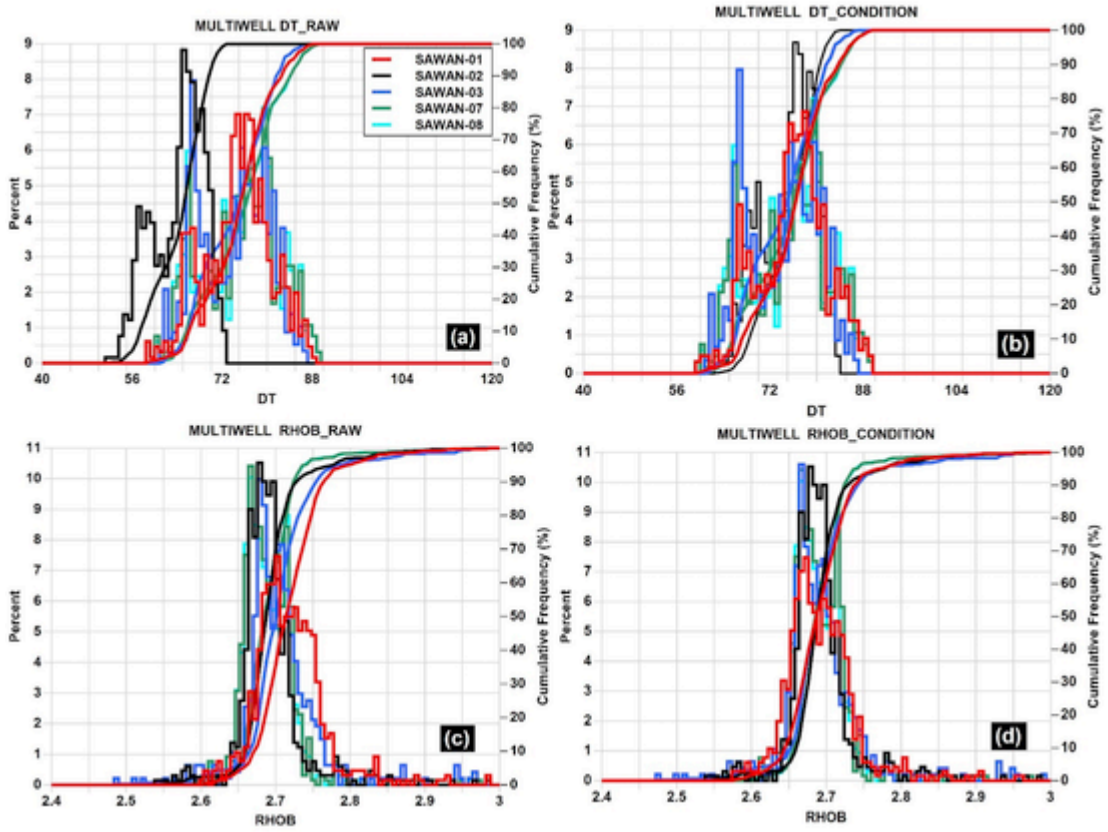

Fig. 4. QC density logs in the wells before and after editing. The top row of the figure shows sonic histograms of raw (a) and conditioned (b) data for each well. The 2nd row of the figure shows density histograms of raw (c) and conditioned (d) data for each well.

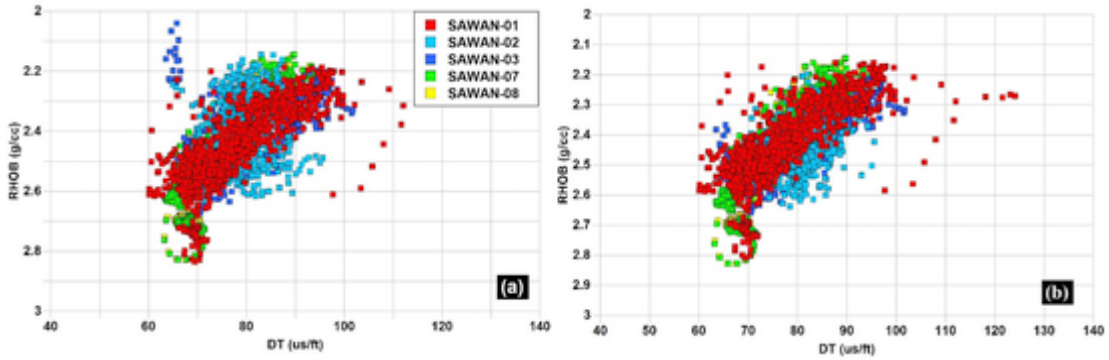

Fig. 5. The crossplot between the density and DT. (a) shows the relationship between the density and DT before correction; Whereas, (b) shows the improved and consistent relationship of density and DT after correction.

Where GR_{max} = are gamma-ray, 100% shale, $GR_{min,}$ = 100 clean sand, respectively (API units), and GR_{log} = gamma-ray log reading in the zone of interest.

Some geophysicists presume that the shale index equals the shale volume, but this overestimates the volume of shale. Thus, a robust relationship is established for diverse geological areas and ages to provide more accurate estimates of shale volume. Clavier et al. (1971) develop a relationship for calculating the accuracy of volume of shale (V_{sh}) in the formation;

$$V_{Sh} = \left[1.7 - \left(I_{GR} + 0.7\right)^2\right]^{\frac{1}{2}} \quad (3)$$

3.2.2. Formation porosities

The sensitive nature of porosity and, then, lithology measurements make the density log a reliable tool to measure sensitivity of porosity (Atlas, 1995). Since the Lower Goru Formation is very heterogeneous because of the presence of the thin layers of sands. Therefore, the existence of these shale layers affects the porosity.

Following equations were employed to eliminate the shale effect for porosities (Eqs. (4) and (5));

$$\emptyset_T = \frac{\rho_{ma} - \rho_b}{\rho_{ma} - \rho_f} \quad (4)$$

Where, $\emptyset_T$ refers total porosity, ρ_{ma} = density of matrix, ρ_b = bulk density, ρ_f = density of fluid.

Density log will measure the effective porosity ($\emptyset_{eff}$) calculated as follows:

$$\emptyset_{eff} = \emptyset_T - v_{sh} * \frac{\rho_{ma} - \rho_{sh}}{\rho_{ma} - \rho_f} \quad (5)$$

Where, Vsh = volume of shale, ρ_{ma} = matrix density, ρ_{sh} = shale density, ρ_f = fluid density.

3.2.3. Water saturation

It is the important petrophysical parameter which quantifies the concentration of hydrocarbons in the reservoir. There are many numbers of methods available that are employed to determine water saturation (*Sw*). The methods most frequently utilized in the gas and oil industry to estimate the water saturation (*Sw*) of field observations (Alao et al., 2013; Widarsono, 2012). For shaly sand formations, Indonesian model (Leveaux et al., 1971) is used to compensate shale effects by using an equation (Eq. (6)):

$$S_w = \left[\frac{V_{sh}^{1-(v_{sh}\times 0.5)}}{\left(\frac{R_{sh}}{R_t}\right)^{0.5}} + \left(\frac{R_t}{R_o}\right)^{0.5}\right]^{\frac{-2}{n}} \quad (6)$$

where V_{sh} = volume of shale, R_{shl} = deep resistivity reading in adjacent shale; R_t = true formation resistivity, $R_o = \frac{\alpha \times R_w}{\emptyset_e^m}$, α = 1 and 0.62 for shale and sandstone, m = *2* and 2.15 for shale and sandstone, and n = *2*.

3.3. Calibration of rock physics model

Various seismic parameters, such as density, Vp, and Vs are controlled and influenced by various aspects. These parameters incorporate pore fluids, lithofacies, pressure, temperature, porosity, and anisotropy, respectively (Wang, 2001). These parameters are very vital to address because they utterly affect the seismic properties. Henceforth, it is of utmost importance to comprehend the relationship amongst these factors and seismic elastic parameters to construct a comprehensive rock physics model. The relationship between porosity and velocity is an effective method because both reservoir and elastic properties are associated with it (Wang, 2001). In an unconsolidated and consolidated reservoir, the relationship of porosity-velocity has various trends and has characteristics of grain-supported sandstones. Commonly, porosity and clay content are the two foremost reasons which are held accountable for the variation in the velocity within the consolidated sand reservoirs. Whereas, in an unconsolidated sand reservoir, cementation ratio, sorting of grains, and sedimentation history are the primitive factors which cause the variation in the velocity (Vernik, 1997). Numerous researchers have made essential tools amid elastic and reservoir parameters. These parameters include clay content and porosity determination (Han et al., 1986), lithofacies (Greenberg and Castagna, 1992), pore fluid types (Batzle and Wang, 1992; Wang et al., 1990), and diagenesis (Dvorkin and Nur, 1996). The mentioned relationships helped us in calibrating a suitable rock physics model. Fig. 6a displays the critical porosity model for the sandstone reservoir in an improved form of a linear interpolation between bulk (K) and shear (G) moduli which shows that $\emptyset = 0$, and $\emptyset = \emptyset C = 38\%$ (Nur et al., 1998). The critical rock porosity distinguishes the load-bearing sediments (at $\emptyset < \emptyset_C$) and suspensions of sand (at $\emptyset > \emptyset C$) (Mavko et al., 2009). Whereas, the porosity-VpVs relationship was to distinguish the consolidated and unconsolidated rocks at $\emptyset_C$ (Fig. 6b).

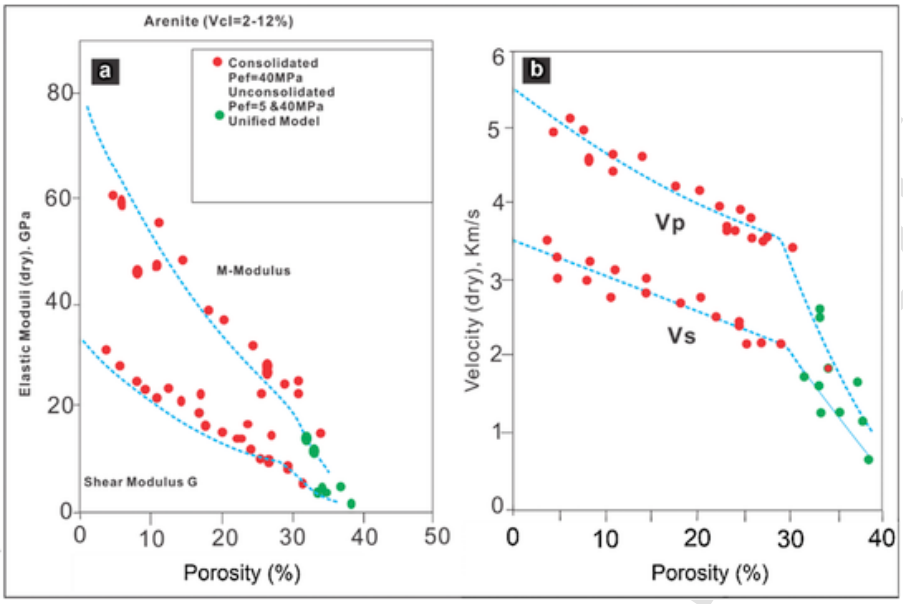

Fig. 6. part (a) of the figure compares the dry elastic moduli with porosity. While part (b) shows the comparison between the dry velocities and porosity for clean unconsolidated and consolidated sand. The Models show an abrupt shift point in porosity at 30% (Vernik, 1997).

3.3.1. Rock physics methodologies

The initial phase builds a rock physics template is determining the suitable rock physics model. The primary methods used in the research are;

3.3.1.1. Shear velocity prediction A general method developed by Greenberg and Castagna (1992) to predict the shear waves (Vs) velocity in water-saturated porous rocks by using compression wave velocity (Vp). The approach assumed that *Vs* is calculated by average arithmetic and harmonic means of the compressional velocities and pure porous lithology (Eq. (7)):

$$V_s = A_2 * V_P^2 + A_1 * V_P + A_0 \tag{7}$$

Vs and *Vp* are the composite rock's shear and compressional wave velocity. A_0, A_1 and A_2 are the empirical coefficients defined in Table 1.The shear wave velocity is missing in wells Sawan 01, Sawan-02 and Sawan-07. At reservoir level in these three wells the missing shear velocities are generated by using Greenberg and Castagna technique, along with Eqs. (8) and (9), which are employed in rock physic modeling.A model developed by Raymer et al. (1980) to calculate compression wave (*Vp*) velocity in porous brine water-filled rock from porosity, compression wave velocity, and solid respectively:

$$V_p = (1 - \emptyset)\, 2V_{ps} + \emptyset\, V_{pf} \tag{8}$$

Later, Dvorkin (2008) used the Raymer model for porous multi-mineral rocks and estimated the shear wave velocity (*Vs*):

Table 1
Representative regression coefficients for shear-wave (VS) versus compressional wave (VP) velocity in pure porous lithologies (Greenberg and Castagna, 1992).

Lithology	A_0	A_1	A_2
Sandstone	−0.85588	0.80416	0
Limestone	−1.03049	1.01677	−0.05508
Dolomite	−0.07175	0.58321	0
Shale	−0.86735	0.76969	0

$$V_s = (1 - \emptyset)\, 2V_{soild} \sqrt{\frac{(1 - \emptyset)\, 2\rho_s}{(1 - \emptyset)\, 2\rho_s + \emptyset\, \rho_f}} \tag{9}$$

where: ρ_f, ρ_s are fluid, solid densities, and $V_{soild}$is the shear velocity of the solid phase, respectively.

3.3.1.2. Matrix (solid) phase Most rocks typically consist of more than a single mineral. Every mineral owns the elastic properties. In this scenario, a perfect solution is to develop individual elastic properties that contain characteristics of elastic minerals of all constituent. There are several approaches to combine various pure minerals with their recognized volumetric fractions (Avseth and Bachrach, 2005). We used Voigt (1910), Reuss (1929) (Eqs. (10) and (11)), and Voigt-Reuss-Hill (RSH) average (Eq. (12)) to measure matrix moduli (Mavko et al., 2009).

$$M_V = \sum_{i=0}^{N} f_i M_i \tag{10}$$

$$\frac{1}{M_R} = \sum_{i=0}^{N} \frac{f_i}{M_i} \tag{11}$$

Where Voigt upper bound on the effective elastic modulus, $M_V$of a mixture of *N* materials (Avseth et al., 2005), f_i is the volume fraction and M_i is the elastic modulus of the ith constituent and Reuss lower bound of the effective elastic modulus, M_R.

$$M_{VR} = \frac{1}{2}(M_V + M_R) \tag{12}$$

Where M_{VR} **Is** Hill's average model denotes the mean value of both Reuss and Voigt.

3.3.1.3. Fluid properties In the reservoir, seismic parameters are mainly affected by the properties of pore fluid. Batzle and Wang (1992) provide a theoretical model and empirical model to estimate the properties of fluid of the three different primary classes of pore fluids: brine, gas, and oil. Hence, the modeling is utilized to compute the properties of fluid of each phase separately.

3.3.1.4. Fluid mixing In the study, the patterns of saturation are known as heterogeneous. Hence, the Wood's average defines the fluids mixture for an effective bulk modulus (Eq. (13)) because it describes the het-

erogeneous pattern of saturation, which is the case in our study area. The following equation was used:

$$\frac{1}{K_{fluid-av}} = \frac{S_{br}}{K_{br}} + \frac{S_{oil}}{K_{oil}} + \frac{S_{gas}}{K_{gas}} \quad (13)$$

where $K_{fluid-av}$ = effective fluid bulk modulus, K_{br} = brine bulk modulus, S_{br} = brine saturation, K_{oil} = oil bulk modulus, S_{oil} = oil saturation, K_{gas} = the gas bulk modulus, S_{gas} = gas saturation and S_w = water saturation.

3.3.1.5. Fluid substitution Gassmann's equation is utilized to estimate properties of elastic attributes at the desire saturation environments, from either dry rock or a rock saturated with different fluids. Generally, fluid substitution begins along the initial group of density and velocities that shows the in-situ rocks with first fluids are known as fluid-1. Fluid substitution workflow is defined by Avseth et al. (2005). Shear moduli and in-situ bulk modulus from P-sonic and S-sonic, and density logs are calculated by using the equations which are as follows:

$$K_{sat1} = \rho_1 \left(V_{p1}^2 - \frac{3}{4} V_{s1}^2 \right)$$

and

$$G_{sat1} = \rho_1 V_{s1}^2$$

The Gassmann equation was employed with the following equations to transform the bulk modulus:

$$\frac{K_{sat2}}{K_s - K_{sat2}} - \frac{K_{fl2}}{\emptyset \left(K_s - K_{fl2} \right)} = \frac{K_{sat1}}{K_s - K_{sat1}} - \frac{K_{fl1}}{\emptyset \left(K_s - K_{fl1} \right)}$$

where $K_{sat1}$and $K_{sat2}$are the rock bulk moduli saturated with fluid-1 and fluid-2, and *Kfl1* and *Kfl2* are the bulk moduli of the fluid-1 and fluid-2 (to be determined).Fluid does not have any resistance to shear deformation according to Gassmann's model; hence, the Saturated effective shear module (G_{sat1}) and (G_{sat2}) are same:

$$G_{sat1} = G_{sat2}$$

The bulk density for the fluid are corrected:

$$\rho_{sat2} = \rho_{sat1} + \emptyset \left(\rho_{fl2} - \rho_{fl1} \right)$$

The new velocities with new fluid are:

$$V_{P\_sat2} = \sqrt{\left(\frac{K_{sat2} + 4/3 G_{sat2}}{\rho_{sat2}} \right)}$$

and

$$V_{S\_sat2} = \sqrt{\left(\frac{G_{sat2}}{\rho_{sat2}} \right)}$$

3.3.1.6. Elastic bounds The Hashin-Shtrikman bounds (HSB) (Hashin and Shtrikman, 1963) and Voigt-Reuss (Reuss, 1929; Voigt, 1910) between the fluid and solid endpoints are measured and are employed to explain different fluid mixtures and physical limitations of diverse minerals. The modified upper Hashin-Shtrikman bound (MUHSB) is applied with high porosity (critical porosity (∅c) = 0.4).

3.3.1.7. Rock physics model and template At the reservoir level, certain contact theory models such as Constant cement models, Contact-cement, and Friable-sand, Stiff sand, models (Mavko et al., 2009), have been tested and evaluated. This model was employed to regenerate *Vp, Vs,* and density, and was correctly compared to the measured data at the location of wells. Hence, Stiff sand (consolidated) model is employed in our study and controlled by localized geological environment to develop a suitable rock physics template.

4. Result and discussion

4.1. Petrophysical properties

The help of elastic logs determines Petrophysical property such as porosity. Hence, logs conditioning plays a vital role in enhancing the quality of the logs that play a role in improving the petrophysical property results. Other reservoir properties such as S_w and V_{sh} are determined by employing a density/neutron crossplot, gamma-ray, and resistivity log. Therefore, we used density/neutron crossplot and gamma-ray logs to calculate shale volume. (Fig. 8).

Density log was used to estimate the total porosity of the reservoir, and on the other hand, a combination of neutron/density log cross-plot are used in all wells, as shown in Fig. 7, and the obtained values are used in the calculation of the shale porosity. The information of the matrix structure indicates that the Lower Indus Basin mainly consists of quartz mineral. Based on Table 2, the density matrix of sandstone is 2.65 g/cm^3. The structure of the Lower Indus Basin shows that clay is present in the form of illite based on the values listed in Table 2, which is obtained in the initial value of Dry Clay Matrix (DCL). The density of the fluid amount used in the study is 1 g/cm^3 (freshwater).

The value of the wet clay matrix density obtained from the cross-plot between neutron-density log is shown in Fig. 7. The density-neutron log cross-plot aimed to obtain the value of DCL and the value of RHOB and NPHI of shale, which will be used to calculate the shale porosity. In Fig. 7(a and b), DCL values of NPHI (0.32, 0.34) and RHOB (2.79 g/cm^3) are obtained. While in Fig. 7 (c and d), the obtained values for DCL are derived from NPHI (0.33 and 0.31) with RHOB (2.78 and 2.79 g/cm^3). These values are used in shale porosity calculation. The differences in values are based on the distinction of a parameter used, which started from the computation of the volume of shale. Fig. 8 shows the estimated total and effective porosity in all wells. The results show that in a good quality interval within the reservoir, the average porosity is about 20–24%. The total and effective porosity is almost equal, especially in the reservoir due to the low amount of shale.

Since to estimate water saturation, Indonesian's equation was employed. Archie's equation parameters a, m, and n applied for Sawan wells are shown in Table 3. For each wells saturation results are shown in Fig. 8. The upper portion of the reservoir shows less water saturation, and the lower part fluctuates between hydrocarbon and water-saturated in each and every well.

4.2. Shear velocity prediction

Shear velocity prediction is the primary goal after petrophysical properties, QC, and data conditioning. The estimated shear velocities in three wells show a complete uniformity and there is a high correlation found in two other wells, see Fig. 9.

4.3. Quality control data

In rock physics analysis, the second step after Vs prediction is quality control of elastic logs. Generating a relationship between petrophysical and elastic properties is a strong tool that helps in quality control logs quality. In several projects for rock physics. Cross-plot is the finest quality control tool with the most unaffected domains to know the quality of the reservoir being shear velocity versus compressional-velocity (*Vs-Vp* domain) and compressional velocity versus density *(Vp-RHOB domain).*

To separate lithology, only using the compressional velocity lonely is not sufficient because of overlapping velocities of the rock. To

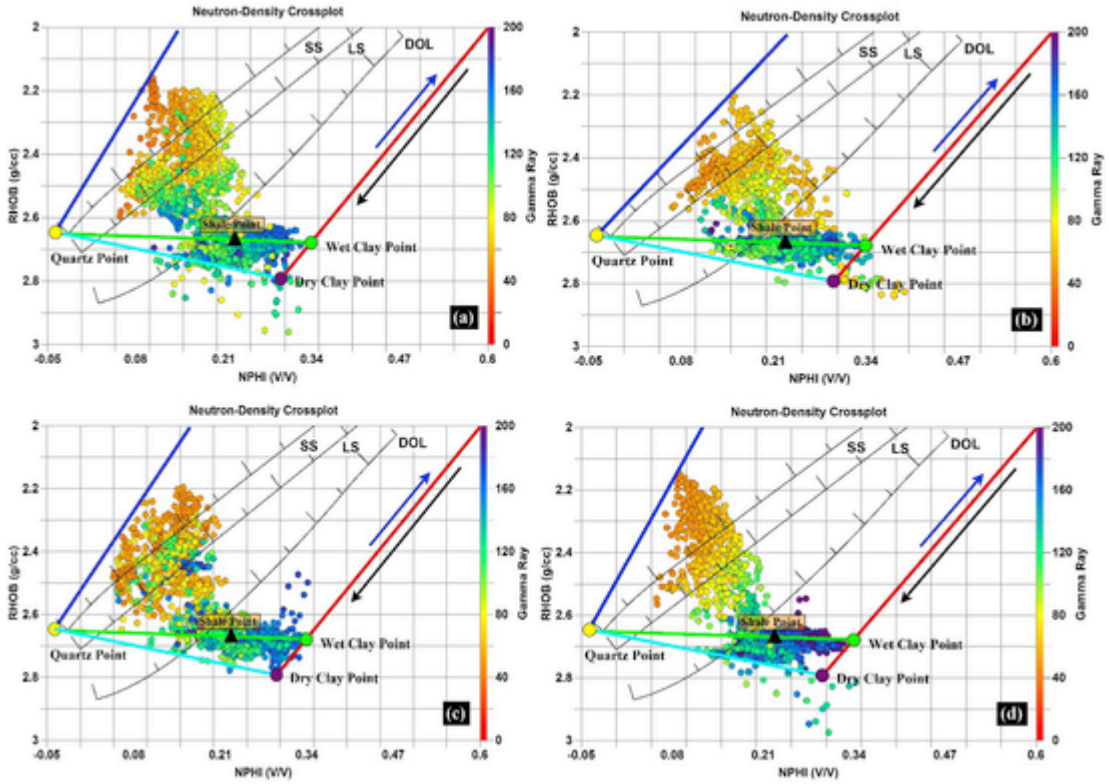

Fig. 7. Neutron/Density crossplot use to selected wet and dry clay points for each well.

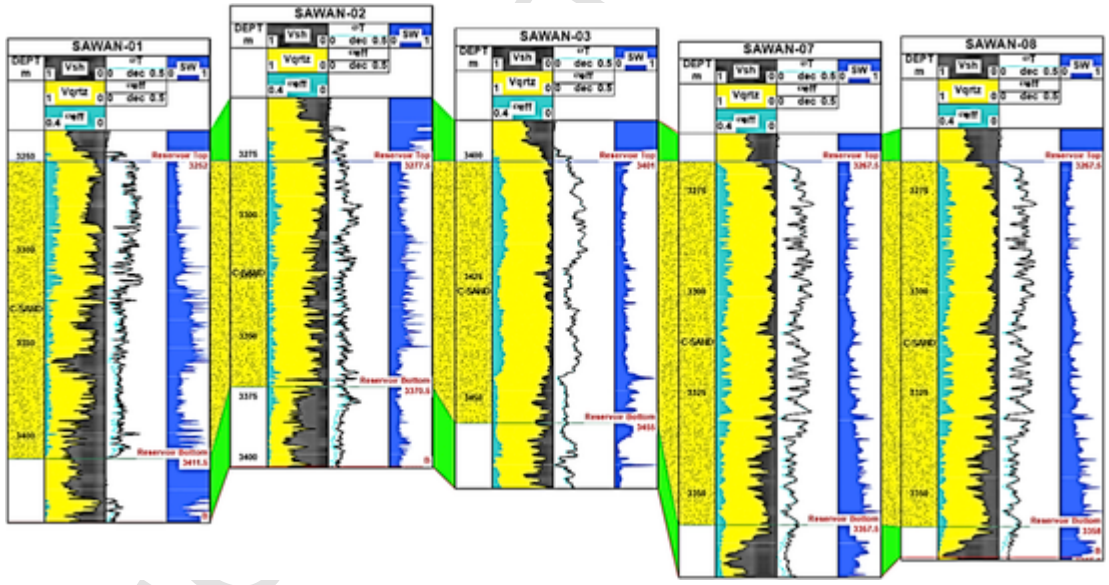

Fig. 8. Estimated water saturation, porosity, and volume of shale for every well (See from left to right).

Table 2
Response matrix tool against mineral log (source: Hughes, 1996).

Lithology	RHOB Density (g/cc)	Neutron logs NPHI (v/v)
Quartz	2.65	−0.04-0
Calcite	2.71	0
Dolomite	2.86	0.04

Table 3
Parameters of Archie for the research area.

Reservoir	a	m	n
Sawan-01	0.65	1.9	2
Sawan-02	0.65	1.8	2
Sawam-03	0.65	1.9	2
Sawan-07	0.65	1.9	2
Sawan-08	0.65	1.9	2

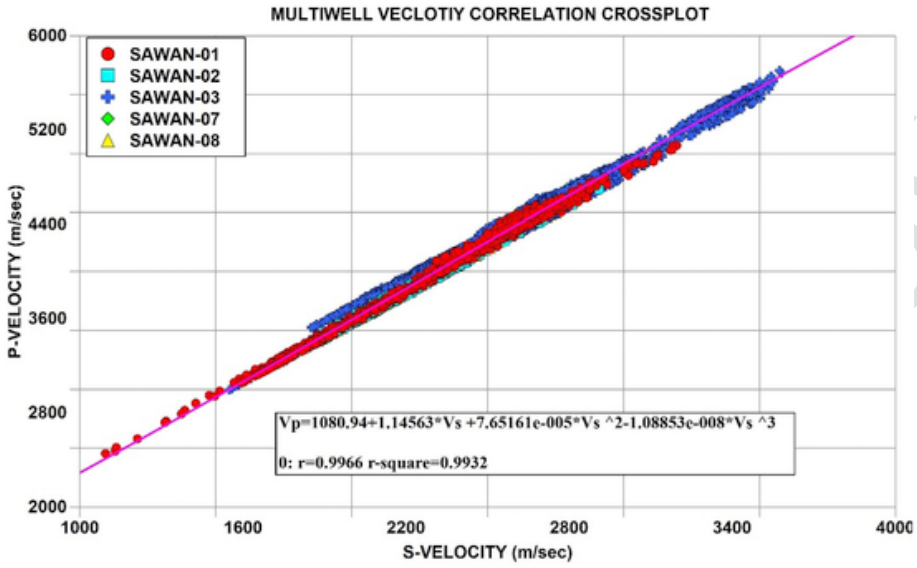

Fig. 9. A comparison between measured and predicted S- velocity (Vs) for all wells.

know about rock composition or deduce uncertainty in the identification of lithology, shear velocity information must be added to compressional velocity data. The Vp-Vs cross-plot at the reservoir levels never included essential details as the reservoir in the study area comprises of heterogeneous sand and shale, (Fig. 10).

The best indicator often used to identify lithology, porosity, and saturation is *the* compressional velocity versus density *(Vp-RHOB* domain) (Avseth et al., 2005; Chi and Han, 2009). The low velocity and density that is similar to the low value of P-impedance generally indicate porosity high value, as shown in Fig. 11. This plot is employed as an indicator of saturation also, while the data is colored by Sw. Such reservoir is categorized as Stiff sand, the saturation effect on both density and velocity plane is generally lesser than the porosity effect. Hence, the interpretation of fluid saturation could be complicated. Fig. 11 indicates that mostly hydrocarbon zone occurs where P-impedance intervals are low.

Eventually, the crossplot compares the P-impedance (*IP*) with velocity ratio that indicates an excellent pointer for the quality of rock, saturation, and lithology. Low *Vp/Vs* and *IP* generally indicate hydrocarbon zones and high-quality data. In our situation, the sensitiveness of the P-impedance - velocity ratio to saturation is substantially in higher porosity zone, but its sensitiveness decreases in middle to low porosity zone (Fig. 12b). Th porosity cutoff, on the other hand, seems obvious in the P-impedance attribute. It isolates low porosity from high porosity at P-impedance (*IP*) = 9000 (*m/s*g/cc*), as shown in Fig. 12a.

4.4. Solid phase averaging and elastic bounds

Summarized from previously interpreted lithological logs and sections, in the reservoir, the solid matrix is a mixture of shale and quartz only. The elastic bounds, provide a concept related to physical limitations of various mixtures of minerals, are applied to Quality Control the data. Fig. 14 shows that the critical porosities with the Voigt-Reuss bounds, between the endpoints of fluid, solid, and modified upper Hashin-Shtrikman bounds (MHSB), range from 0.1 to 1, which are further superimposed by the in-situ data bulk modulus-porosity in all well. The evaluated data in all well falls within the bounds limit. The cross-plots is indicating that the critical porosity ($\emptyset_c$) is about 0.4 in the reservoir.

The average porosity varies at the reservoir from low to high values. The amount of porosity is low in some zone at shallow and deep intervals of the reservoir. On the other hand, the porosity value is quite high in the middle interval of the reservoir (i.e., 0.25) (Fig. 13).

We apply modified upper and lower Hashin-Shtrikman bounds (MHSB) with a proper minerals endpoint and critical porosity (0.4) that will help to identify QC data stiffness or softness in the reservoir. The cross-plot of bulk modulus versus porosity, which contains measured-data and modified upper and lower Hashin-Shtrikman bounds in Fig. 14 displays the data is falling nearly and through the upper MHSB (solid line), hence describes the data as consolidated (Stiff sand).

4.5. Fluid mixing analysis

The density and bulk modulus of water are functions of temperature, pressure, and salinity (Murphy et al., 1993). The hydrocarbon, gas, and oil properties are more variable and highly dependent on temperature and composition (Murphy et al., 1993). For reservoir conditions, Batzle and Wang (1992) is utilized to recalculate fluid properties. Table 4 lists the properties of fluid input and output.

Fig. 15 shows the results of fluid mixtures between water and gas. On the behavior of elastic properties, the existence of less amount of gas in the fluid system shows considerable effects. In our situation, the existence of gas significantly decreases the P-Impedance in the fluid system.

4.6. Fluid substitution analysis

Afterward determining fluid, solid properties, and predicting shear velocities, Gassmann's model was employed with three sets of scenarios to check the presence of oil, gas, and water within the reservoir interval. The three sets of scenarios are as follows;

- 100% brine water-saturated;
- 10% brine and water 90% gas;
- 20% brine water with 80% oil.

Fig. 17 represents models and in-situ log according to Gassmann's equation for estimation. Different colors show the different scenarios, red logs show gas and black logs define in-situ (original data), blue logs indicate water. The hydrocarbon is primarily gas at the reservoir level of the Sawan gas field (Fig. 1a). Comparison between the gas case (red logs) with in-situ case (black logs), it is concluded that they over-

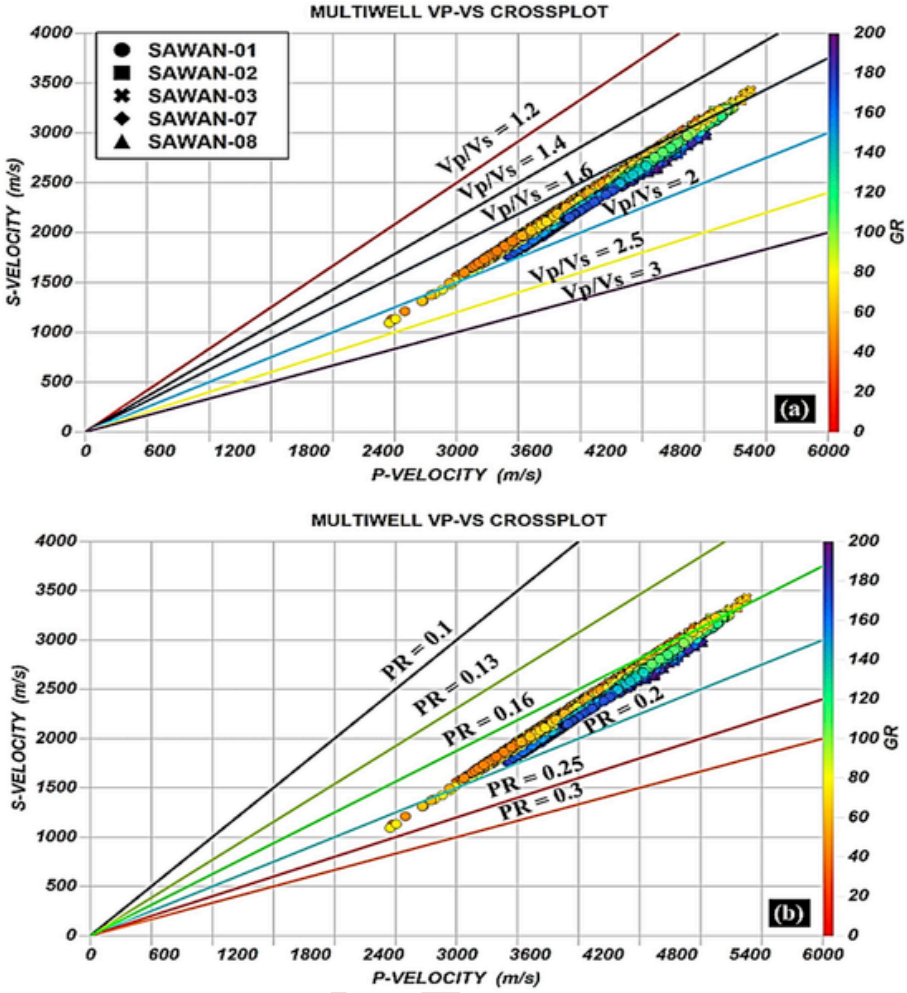

Fig. 10. The cross plots show P-Velocity vs. S. Velocity with color-coded GR. The Cross-plot (a) at the top is superimposed by Vp/Vs and Cross-plot (b) at the bottom is superimposed by poisson's ratio. (For interpretation of the references to color in this figure legend, the reader is referred to the Web version of this article.)

lay each other at the reservoir level representing high water saturation. The division among diverse scenarios is essential in numerous elastic attributes (e.g., Lambda-rho, Lambda/Mu, and *Vp/Vs*), particularly in the high porosity and low water saturation zone (Fig. 17).

The outcomes of Gassmann's fluid substitution in the crossplot of P-impedance versus velocity ratio is shown in Fig. 16. The division among diverse fluid scenarios is noticeable. The range of the gas reservoir within the study area lies between 7000 and 11000 (g/cc*m/s) P-impedance value and 1.5–1.7 *Vp/V* value. Porosity increases in the low P-impedance direction. Whereas, in low-velocity ratio direction, hydrocarbon-saturation increases. The sensitiveness of the *Vp/Vs* ratio to various fluids is usually considerable.

4.7. Rock physics modeling

The outcomes of the different rock physics models applied in the research show that Stiff sand (consolidated) is quite a suitable and reliable rock physics model for the Lower Goru sand reservoir (Fig. 18). Hence, the Stiff sand (consolidated) model was chosen in our study to connect the two endpoints between the modulus-porosity-plane and the upper MHSB.

Th first endpoint is at zero porosity. It shows the average of the mixed minerals among shale and quartz. The second endpoint, at high porosity ($\emptyset_c$), shows the high quartz content, which represents the Stiff sand. Whereas, the data after the critical porosity (0.4) represents that the sand is suspension sand.

4.8. Rock physics template

The Rock Physics Templates (RPTs) is a useful tool for the determination of lithology and fluid prediction (Ødegaard and Avseth, 2004). The primary goal of the RPT analysis using seismic data and well-log is to construct a resourceful rock physics model constrained by the local geology. Avseth et al. (2005), illustrated that the Gassmann fluid substitution model is a useful tool to construct the rock physics models and rock physics templates through depositional and diagenetic trend models. The mentioned method has been successfully applied by the seismic experts (for seismic inversion reservoir characterization), rock physicists (for evaluation of the seismic applicability through well-logs), and Petro-physicists (for the assessment of the formation evaluation). After the rock physics model is calibrated by logging data, the measured P-wave velocity, S-wave velocity, and density logs are matching the modeled log very well (Fig. 19), which shows that the model is appropriate for this research and can be used for further analysis. We can obtain the RPT from the following workflow, firstly, a pseudo well is made, which has a series of different clay volume (0-1), porosity (0–0.25) and water saturation (0-1); then two variables are fixed, and one variable is changed, for instance, when we want to know how does the clay volume affect the elastic parameters, the porosity, and water satu-

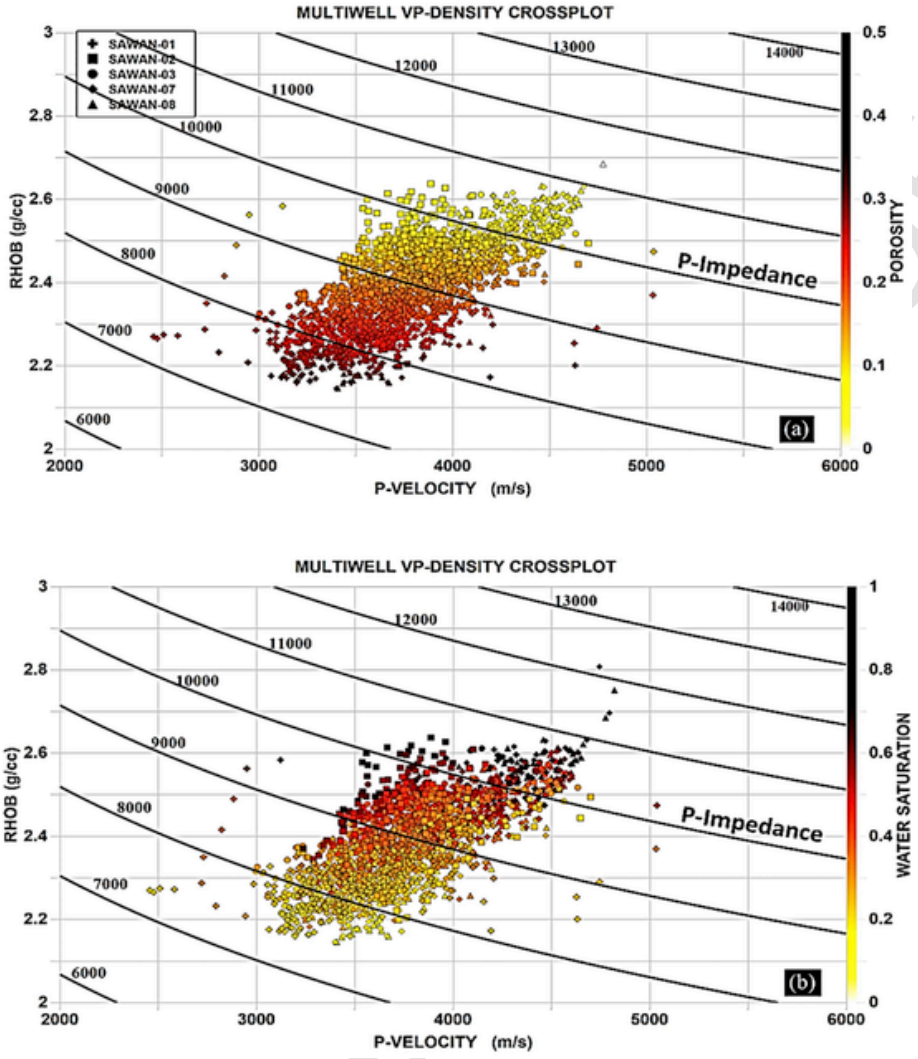

Fig. 11. P-Velocity vs. density for each and ever well colored with porosity and water saturation; superimposed by P-impedance.

ration curve will set to be a constant, and then, these three curves are input into the calibrated model. The Vp, Vs, and density curve under different shale content, porosity, and water saturation is obtained. Finally, the cross plot of velocity ratio versus P-impedance, color-coded with porosity are made (Fig. 20a); and color-coded with volume of Vclay (Fig. 20b). The scattered point represents the logging data. This shows the accuracy and feasibility of the calibrated RPT for this study.

After analyzing the validity of the model-predicted, it is determined and confirmed that the RPD is based on the in-situ data at the well sites. The next phase employs the model based on seismic-elastic attributes to predict petrophysical properties. The study focuses on finding porosity from the seismically derived impedance. Hence, the study uses the best second-order polynomial regression (Eq. (14)) to relate the porosity with a measured impedance that is generated to distinguish the sand from shale in a single rock physics cross plot, validated with shale volume (Vsh) (Fig. 21). Cross plotting shows that acoustic impedance is reasonably correlated with the porosity of both the lithologies. Rock physics diagnostic confirms the fact that porosity slope tends to be steep when it is controlled by diagenesis and flat when porosity is controlled by grain size for different lithologies (Mavko and Mukerji, 1998).

$$\text{POROSITY} = 12276.2 - 18091 * \text{P} - \text{Impedance} \quad (14)$$

5. Conclusion

The research focuses on developing a rock physics model and template to diagnose a consolidated sand reservoir. A rock physics modeling and integrated petrophysical evaluation methods are employed to calculate the reservoir properties of Lower Goru sand reservoir, Pakistan. The formulated approach gives an idea to generate a perfect and persistent rock physic model. The Stiff sand model indicates the best uniformity among calculated and modeled velocities. The correlativity among the measured and modeled velocities of Vp and Vs wave is 99.26% and 99.97%, respectively.

In the research area, a perfect coherency of modeling laid a substantial base for enhanced reservoir characterization. The measured model also proves to be useful in precisely calculating the elastic logs such as Vp, Vs, and density in all wells. The quantitative values of cross plots, such as the average cutoff of petrophysical and elastic parameters, describe an ostensible differentiation among shale, shaly sand, and gas-bearing sand zones. The results identify that in gas-bearing sand, the VP/VS ratio is much sensitive, followed by P-impedance.

The proposed model and calibrated RPT can be used to enhance seismic reservoir properties. The reliability of the model is helpful for the formation evaluation, reservoir characterization, and prospect evaluation across different fields of the Lower Goru sand reservoir. The pre-

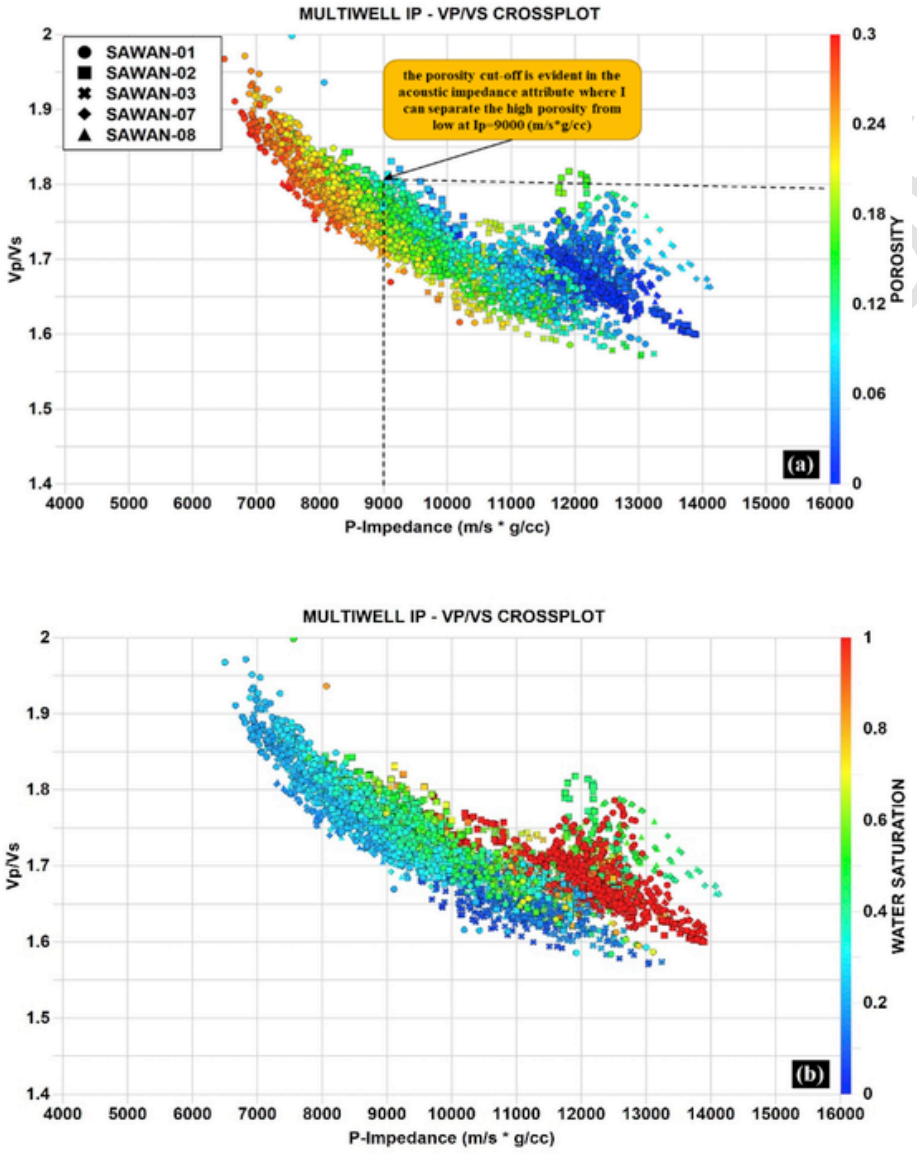

Fig. 12. (a) compares the P-impedance with velocities for all wells, colored with porosity. Whereas, (b)shows a comparison between P-impedance and velocities for all wells, colored with Water saturation.

dicted model can further be utilized to estimate porosity from the seismically derived impedance worldwide that has the same geological trends and reservoir distribution.

Credit author statement

Conceptualization, M.A.; methodology, M.A.; software, M.A.; validation, M.A.; formal analysis, M.A.; investigation, M.A.; resources, M.A.; data correction, M.A.; writing-original draft, M.A.; and writing-review editing, M.A.; ,M.H.; visualization, supervision, M.H.; , M.P.;,R.J.; , U.M.; project administration, funding acquisition, M.H.; , M.P.

Declaration of competing interest

The authors do not have any conflict of interest to declare.

Acknowledgments

I am thankful to the oil and gas Ministry of Pakistan, for providing the research data and sample. The financial support of this research has been provided by the national key research and Development Program of China (2016YFC0600201), the National Nature Science Foundation of China (Grant No. 41630317).

Appendix A. Supplementary data

Supplementary data associated with this article can be found, in the online version, at https://doi.org/10.1016/j.petrol.2020.107461.

Uncited reference

Ali et al., 2018.

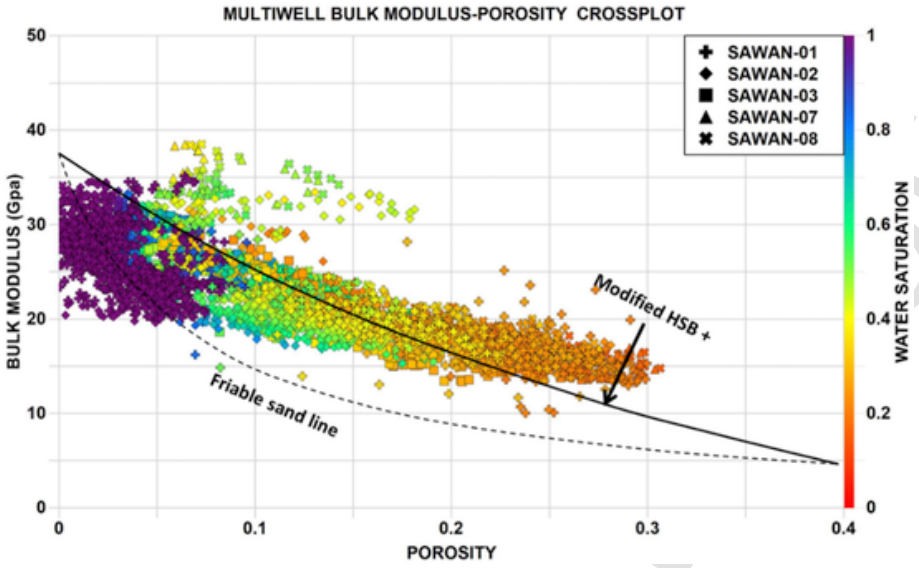

Fig. 13. The upper and lower MHSB at $\emptyset_c = 0.4$ are superimposed by the in-situ data on bulk modulus – porosity domain, colored by GR.

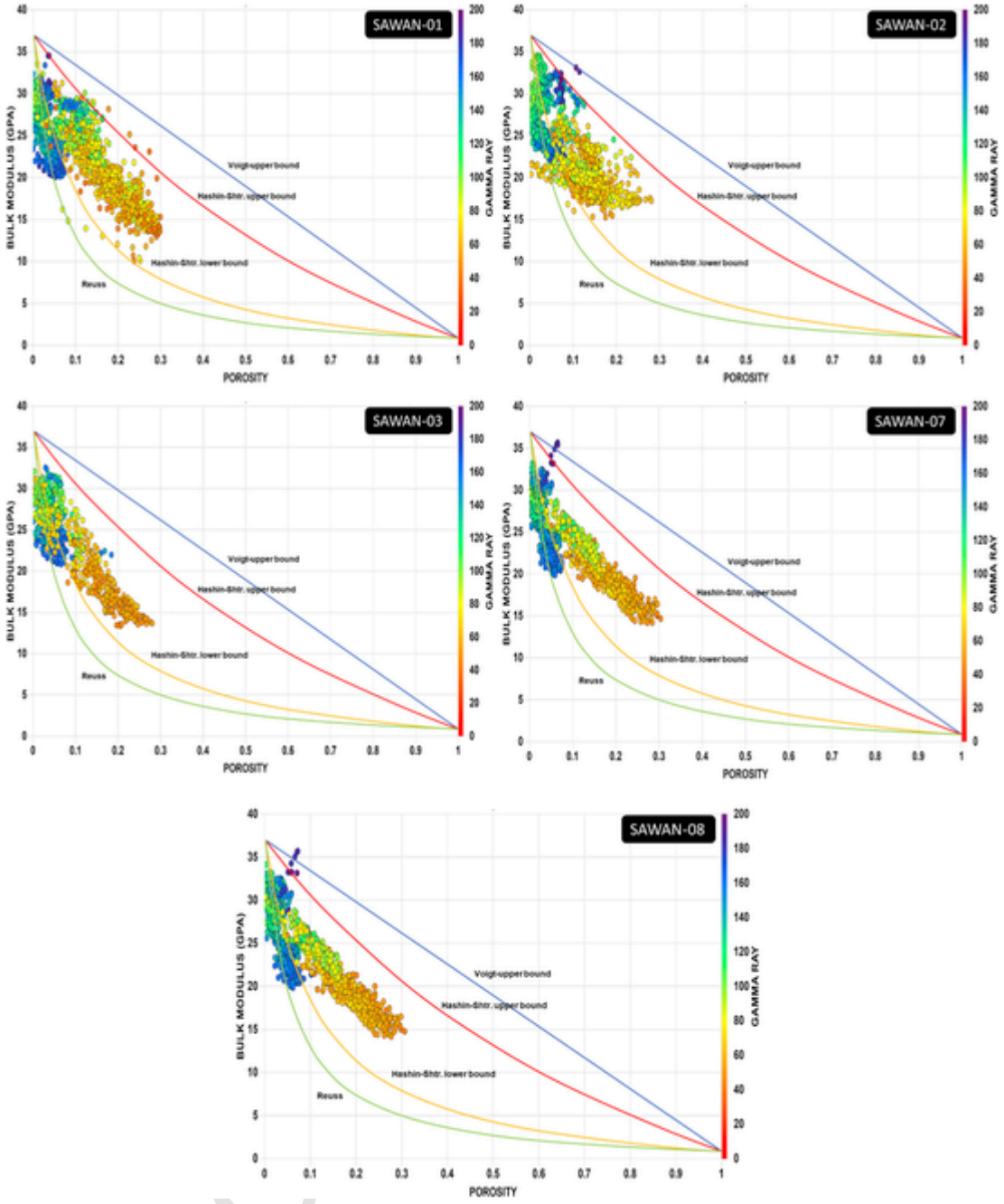

Fig. 14. Voigt-Reuss and upper bounds of Hashin-Shtrikman with various critical porosities range from 0.1 to 1 and are superimposed by the measured data on K-∅ plane, colored by GR.

Table 4
Fluid properties input and output are computed by (Batzle and Wang, 1992).

Input		Output		
Temperature (°C)	174		Brine	Gas
Pressure (Mpa)	37.14	Velocity (m/s)	1357.8	682.8
Gas gravity	0.64	Bulk modulus (GPa)	1.726	0.0798
Salinity (ppm)	30000	Bulk density (g/cm ^{3})	0.9362	0.1711

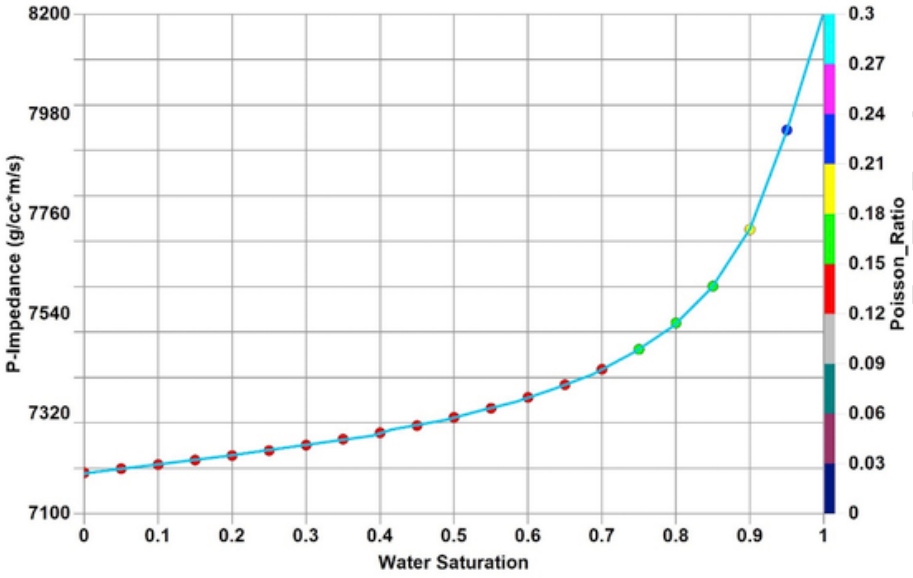

Fig. 15. The results of Fluid mixture are extracted by applying the Wood's equation between water and gas in the water Saturation- P-Impedance area.

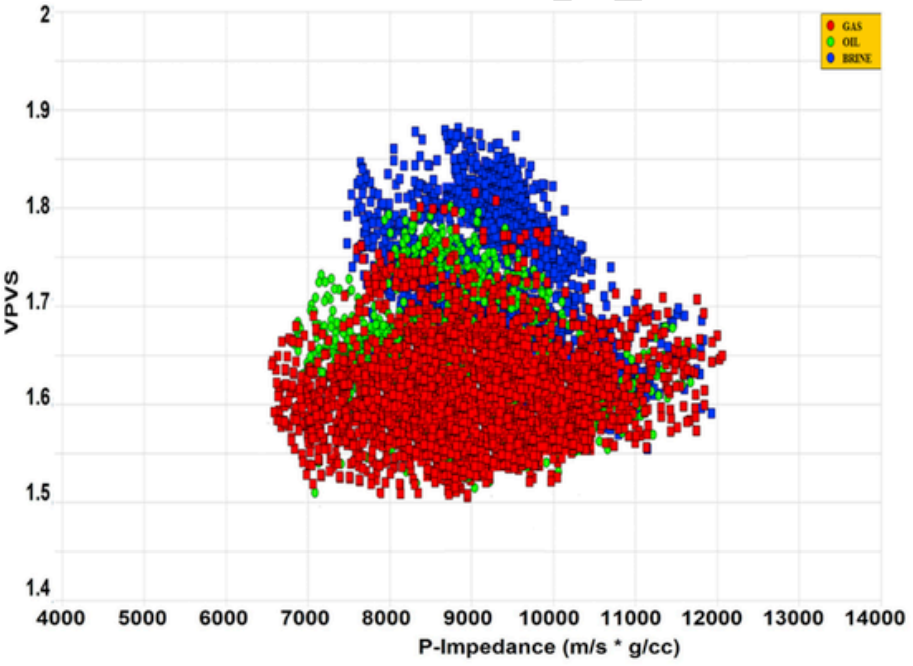

Fig. 16. *P-impedance vs.* velocity ratios *for all wells in three different scenarios.*

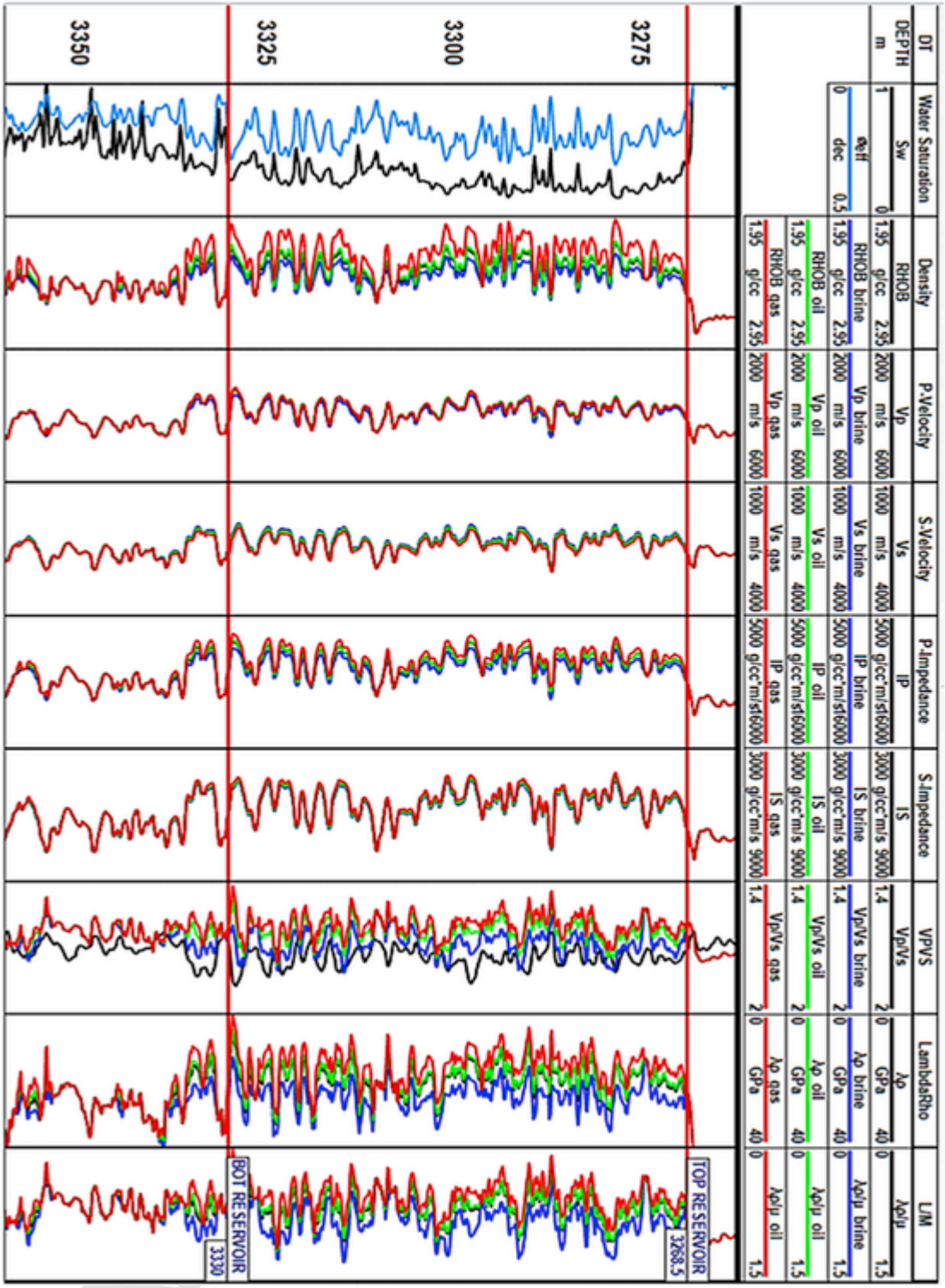

Fig. 17. Results for Sawan-08 well with Gassmann's model (blue log curve for water, red log curve for gas, green log curve for oil, and black log curve for in-situ). (For interpretation of the references to color in this figure legend, the reader is referred to the Web version of this article.)

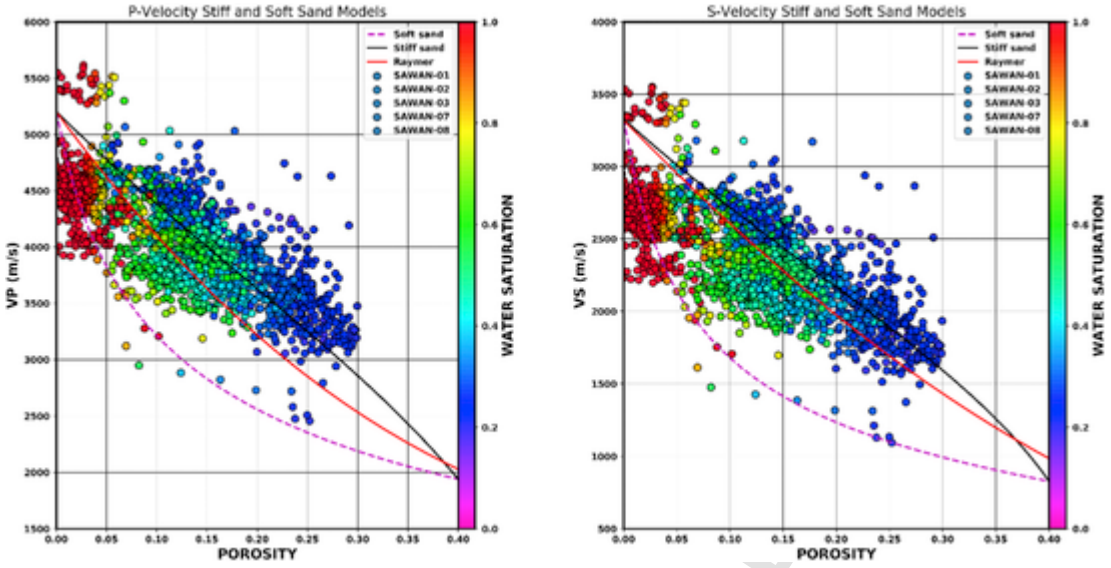

Fig. 18. The cross plot compares the porosity and velocities. It includes the in-situ data for each well that are superimposed by Stiff sand, Friable-sand, Raymer models and shear velocity predictors.

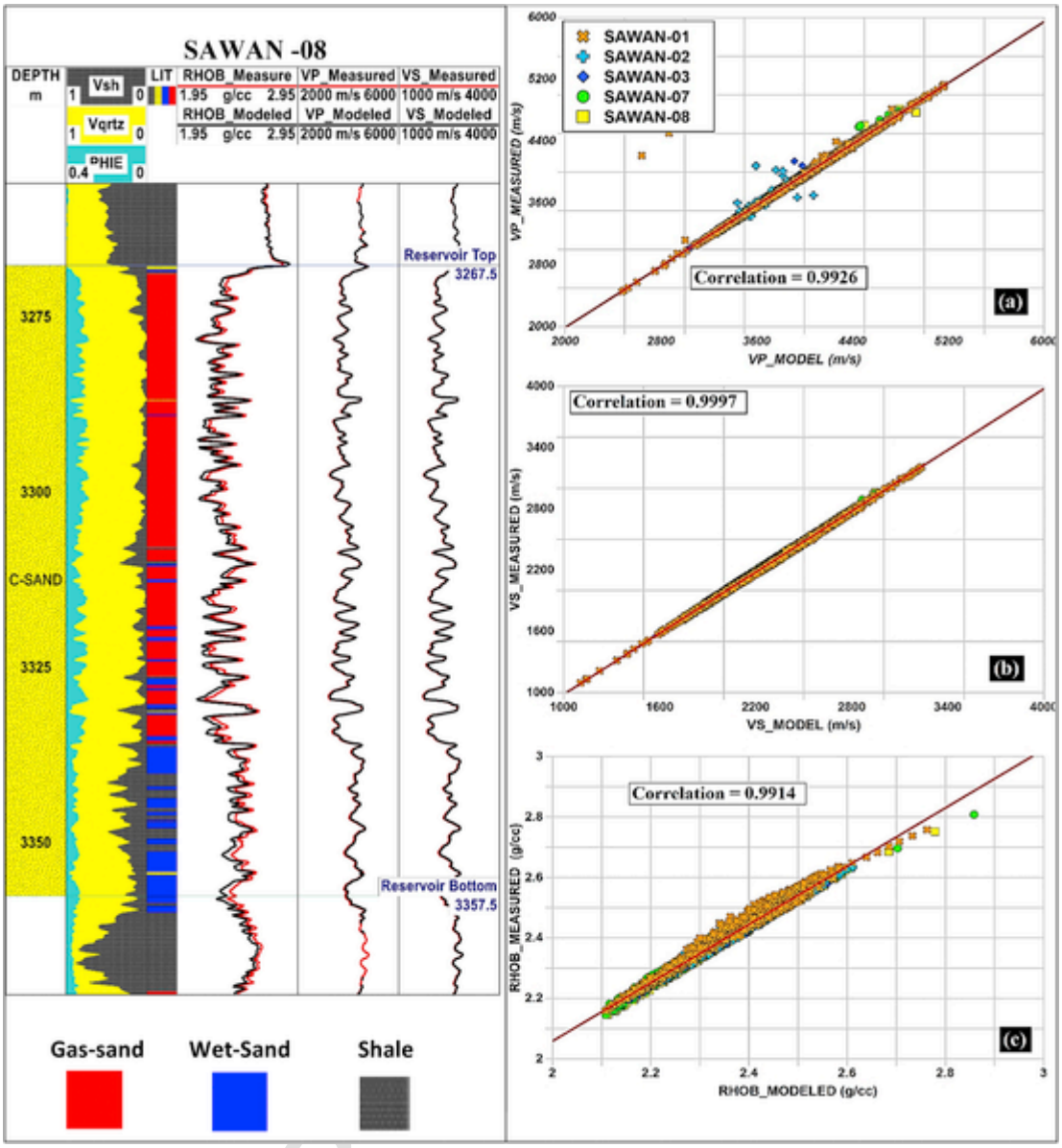

Fig. 19. The elastic modeled data using the Stiff sand model in all wells. Mineralogy, lithology, density, P-velocity, and shear velocity in Sawna-08 (from left to right). The cross plots show correlation between Vp and Vp model (a), Vs and Vs model(b), and density and density model (c).

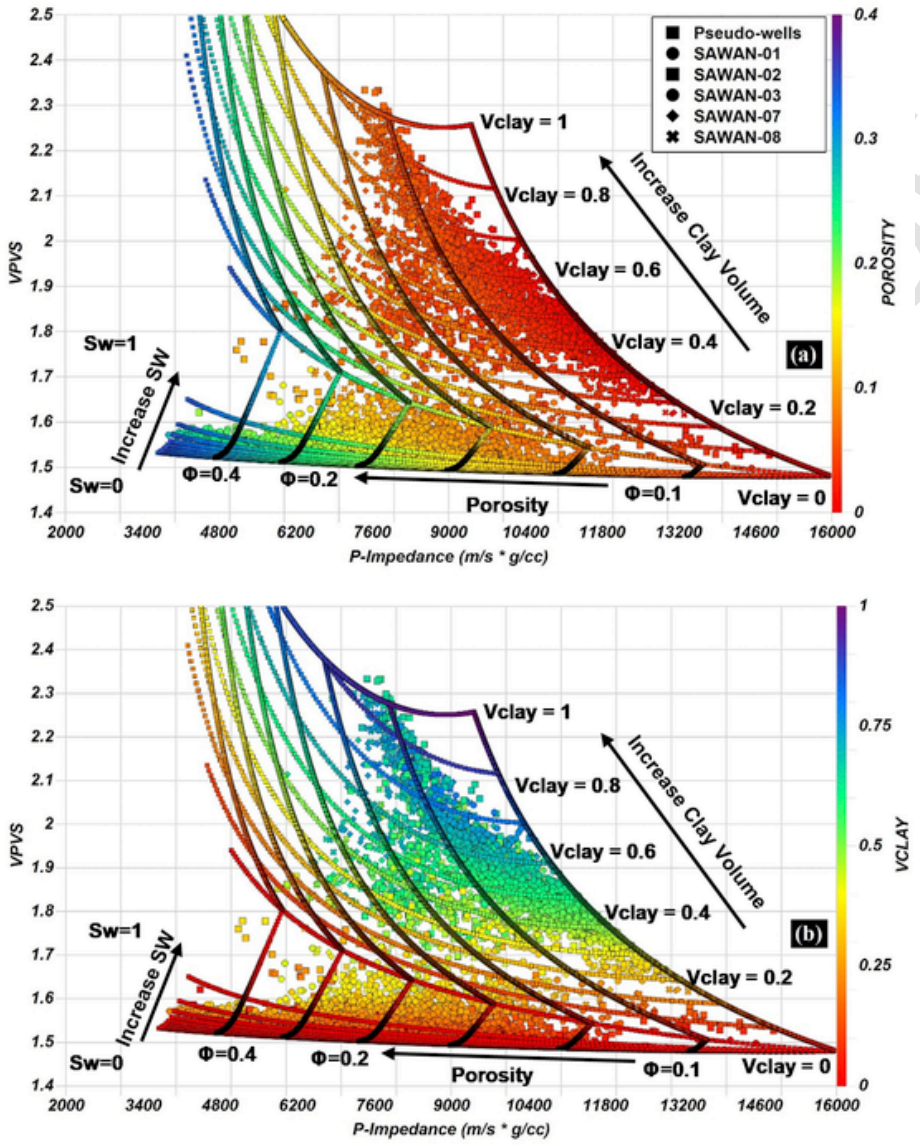

Fig. 20. The novel/calibrated model shows the accuracy of Stiff sand RPT model: (a) RPT colored with porosity and (b) RPT colored with volume of clay.

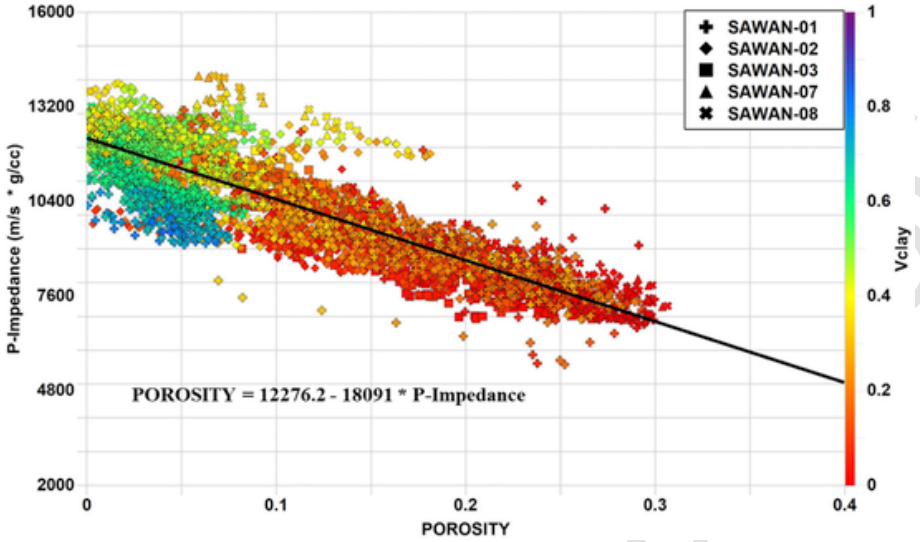

Fig. 21. The crossplot shows the porosity vs. p-impedance includes in-situ data for each and every well, colored with Vclay.

References

Afzal, J, Kuffner, T, Rahman, A, Ibrahim, M, 2009. Seismic and well-log based sequence stratigraphy of the early cretaceous, lower Goru "C" sand of the sawan gas field, middle Indus platform, Pakistan. In: Proceedings, Society of Petroleum Engineers (SPE)/Pakistan Association of Petroleum Geoscientists (PAPG) Annual Technical Conference (Islamabad, Pakistan).

Ahmad, N, Chaudhry, S, 2002. Kadanwari Gas Field, Pakistan: a disappointment turns into an attractive development opportunity. Petrol. Geosci.. doi:10.1144/petgeo.8.4.307.

Ahmad, N, Fink, P, Sturrock, S, 2004. Sequence Stratigraphy as Predictive Tool in Lower Goru Fairway, Lower and Middle Indus Platform. Pakistan. Atc 2004.

Ahmed, N, Khalid, P, Anwar, A W, 2016. Rock physics modeling to assess the impact of spatial distribution pattern of pore fluid and clay contents on acoustic signatures of partially-saturated reservoirs. Acta Geod. Geophys. 51, 1–13. doi:10.1007/s40328-015-0101-0.

Alao, P A, Ata, A I, Nwoke, C E, 2013. Subsurface and petrophysical studies of shaly-sand reservoir targets in apete field, Niger delta. ISRN Geophys. doi:10.1155/2013/102450.

Ali, A, Alves, T M, Saad, F A, Ullah, M, Toqeer, M, Hussain, M, 2018. Resource potential of gas reservoirs in South Pakistan and adjacent Indian subcontinent revealed by post-stack inversion techniques. J. Nat. Gas Sci. Eng.. doi:10.1016/j.jngse.2017.10.010.

Ali, Muhammad, Khan, M J, Ali, Mubarik, Iftikhar, S, 2019. Petrophysical analysis of well logs for reservoir evaluation: a case study of "Kadanwari" gas field, middle Indus basin, Pakistan. Arab. J. Geosci. 12. doi:10.1007/s12517-019-4389-x.

Anees, A, Shi, W, Ashraf, U, Xu, Q, 2019. Channel identification using 3D seismic attributes and well logging in lower Shihezi Formation of Hangjinqi area, northern Ordos Basin, China. J. Appl. Geophys.. doi:10.1016/j.jappgeo.2019.02.015.

Anwer, H M, Alves, T M, Ali, A, Zubair, 2017. Effects of sand-shale anisotropy on amplitude variation with angle (AVA) modelling: the Sawan gas field (Pakistan) as a key case-study for South Asia's sedimentary basins. J. Asian Earth Sci.. doi:10.1016/j.jseaes.2017.07.047.

Ashraf, U, Zhu, P, Anees, A, Abbas, A, Talib, A, 2016. Analysis of balkassar area using velocity modeling and interpolation to affirm seismic interpretation, upper Indus Basin. Geosciences 2016 (6), 78–91. doi:10.5923/j.geo.20160603.02.

Ashraf, U, Zhu, P, Yasin, Q, Anees, A, Imraz, M, Mangi, H N, Shakeel, S, 2019. Classification of reservoir facies using well log and 3D seismic attributes for prospect evaluation and field development: a case study of Sawan gas field, Pakistan. J. Petrol. Sci. Eng. 175, 338–351. doi:10.1016/j.petrol.2018.12.060.

Ashraf, U, Zhu, P, Yasin, Q, Anees, A, Imraz, M, Mangi, H N, Shakeel, S, 2019. Classification of reservoir facies using well log and 3D seismic attributes for prospect evaluation and field development: a case study of Sawan gas field, Pakistan. J. Petrol. Sci. Eng. 175, 338–351.

Atlas, W, 1995. Introduction to Wireline Log Analysis. West. Atlas Int. Inc., Houston, Texas.

Avseth, P, 2000. Combining Rock Physics and Sedimentology for Seismic Reservoir Characterization of North Sea Turbidite Systems. Stanford Univ, p. 181.

Avseth, P, Bachrach, R, 2005. Seismic properties of unconsolidated sands: tangential stiffness, Vp/Vs ratios and diagenesis. In: Society of Exploration Geophysicists - 75th SEG International Exposition and Annual Meeting, SEG 2005. doi:10.1190/1.2147968.

Avseth, P, Mukerji, T, Mavko, G, 2005. Quantitative Seismic Interpretation: Applying Rock Physics Tools to Reduce Interpretation Risk, Quantitative Seismic Interpretation: Applying Rock Physics Tools to Reduce Interpretation Risk. doi:10.1017/CBO9780511600074.

Azeem, T, Chun, W Y, Khalid, P, Qing, L X, Ehsan, M I, Munawar, M J, Wei, X, 2017. An integrated petrophysical and rock physics analysis to improve reservoir characterization of Cretaceous sand intervals in Middle Indus Basin, Pakistan. J. Geophys. Eng. 14, 212–225. doi:10.1088/1742-2140/14/2/212.

Azeem, T, Yanchun, W, Khalid, P, Xueqing, L, Yuan, F, Lifang, C, 2016. An application of seismic attributes analysis for mapping of gas bearing sand zones in the sawan gas field, Pakistan. Acta Geod. Geophys.. doi:10.1007/s40328-015-0155-z.

Batzle, M, Wang, Zhijing, 1992. Seismic properties of pore fluids. Geophysics 57, 1396–1524. doi:10.1190/1.1443207.

Berger, A, Gier, S, Krois, P, 2009. Porosity-preserving chlorite cements in shallow-marine volcaniclastic sandstones: evidence from cretaceous sandstones of the sawan gas field, Pakistan. Am. Assoc. Petrol. Geol. Bull.. doi:10.1306/01300908096.

Berryman, J G, Laboratories, B, 1980. Long-wavelength propagation in composite elastic media I. Spherical inclusions. J. Acoust. Soc. Am. 68, 1809–1819. doi:10.1121/1.385171.

Berryman, J G, Milton, G W, 1991. Exact results for generalized Gassmann's equations in composite porous media with two constituents. Geophysics 56, 1950–1960.

Burch, D, 2002. GC Seismic to Well Ties with Problematic Sonic Logs.

Castagna, J P, Swan, H W, 1997. Principles of AVO crossplotting. Lead. Edge 16, 337–344. doi:10.1190/1.1437626.

Cheng, A, Toksöz, M N, 1979. Inversion of seismic velocities for the pore aspect ratio spectrum of a rock. Geophys. J. F 84. doi:10.1029/JB084iB13p07533.

Chi, X G, Han, D H, 2009. Lithology and fluid differentiation using a rock physics template. Lead. Edge 28, 60–65. doi:10.1190/1.3064147.

Clavier, C, Hoyle, W, Meunier, D, 1971. Quantitative interpretation of thermal neutron decay time logs: Part I. Fundamentals and techniques. J. Petrol. Technol.. doi:10.2118/2658-a-pa.

Dvorkin, J, Nur, A, 1996. Elasticity of high-porosity sandstones: theory for two North Sea data sets. Geophysics 61, 1363–1370. doi:10.1190/1.1444059.

Dvorkin, J, Nur, A, Yin, H, 1994. Effective properties of cemented granular materials. Mech. Mater. 18, 351–366. doi:10.1016/0167-6636(94)90044-2.

Dvorkin, J P, 2008. Yet another V s equation. Geophysics 73, E35–E39. doi:10.1190/1.2820604.

Gardner, G H F, Gardner, L W, Gregory, A R, 1974. Formation velocity and density - the diagnostic basics for stratigraphic traps. Geophysics. doi:10.1190/1.1440465.

Gassmann, F, 1951. On the elasticiy of porous media. Mitteilungen aus dem Inst. fur Geophys. 96, 1–21. doi:10.1190/1.9781560801931.ch3p.

Gray, D, Day, S, Schapper, S, 2015. Rock physics driven seismic data processing for the Athabasca oil sands, Northeastern Alberta. CSEG Rec 32–40 March.

Greenberg, M L, Castagna, J P, 1992. Shear-wave velocity estimation in porous rocks: theoretical formulation, preliminary verification and applications. Geophys. Prospect.. doi:10.1111/j.1365-2478.1992.tb00371.x.

Han, D, Nur, A, Morgan, D, 1986. Effects of porosity and clay content on wave velocities in sandstones. Geophysics 51, 2093–2107. doi:10.1190/1.1893163.

Hashin, Z, Shtrikman, S, 1963. A variational approach to the theory of the elastic behaviour of multiphase materials. J. Mech. Phys. Solid. 11, 127–140.

He, F B, You, J, Chen, K Y, 2011. Gas sand distribution prediction by prestack elastic inversion based on rock physics modeling and analysis. Appl. Geophys. 8, 197–205. doi:10.1007/s11770-011-0285-1.

Hill, R, 1952. The elastic behaviour of a crystalline aggregate. Proc. Phys. Soc. 65, 349.

Hussain, M, Ahmed, N, Chun, W Y, Khalid, P, Mahmood, A, Ahmad, S R, Rasool, U, 2017. Reservoir characterization of basal sand zone of lower Goru Formation by petrophysical studies of geophysical logs. J. Geol. Soc. India 89, 331–338. doi:10.1007/s12594-017-0614-y.

Ismail, A, Yasin, Q, Du, Q, Ali Bhatti, A, 2017. A comparative study of empirical, statistical and virtual analysis for the estimation of pore network permeability. J. Nat. Gas Sci. Eng. 45, 825–839. doi:10.1016/j.jngse.2017.07.002.

Kadri, I B, 1995. Petroleum Geology of Pakistan. Pet. Geol. Pakistan.

Kazmi, A H, Jan, M Q, 1997. Geology and Tectonics of Pakistan. Graphic publishers.

Khalid, P, Broseta, D, Nichita, D V, Blanco, J, 2014. A modified rock physics model for analysis of seismic signatures of low gas-saturated rocks. Arab. J. Geosci. 7, 3281–3295. doi:10.1007/s12517-013-1024-0.

Khan, J M, Moghal, M A, Jamil, M A, 1999. Evolution of shelf margin & distribution of reservoir facies in early cretaceous of Central Indus Basin Pakistan. In: Annual Technical Conference (ATC). pp. 1–23.

Khan, M J, Khan, H A, 2018. Petrophysical logs contribute in appraising productive sands of Lower Goru Formation, Kadanwari concession, Pakistan. J. Pet. Explor. Prod. Technol. 8, 1089–1098. doi:10.1007/s13202-018-0472-1.

Khan, M S, Masood, F, Ahmed, Q, Jadoon, I A K, Akram, N, 2017. Structural interpretation and petrophysical analysis for reservoir sand of lower Goru, Miano area, central Indus Basin, Pakistan. Int. J. Geosci. 379–392 08. doi:10.4236/ijg.2017.84020.

Krois, P, Mahmood, T, Milan, G, 1998. Miano field, Pakistan, A case history of model driven exploration. In: Proceedings Pakistan Petroleum Convention. pp. 112–131.

Kuster, G T, Toksöz, M N, 1974. Velocity and attenuation of seismic waves in two-phase media: part i. theoretical formulations. Geophysics. doi:10.1190/1.1440450.

Leveaux, J, Poupon, A, others, 1971. Evaluation of water saturation in shaly formations. Log. Anal. 12.

Liu, Z, Sun, S Z, 2015. The differential Kuster-Toksï¿½z rock physics model for predicting S-wave velocity. J. Geophys. Eng. 12, 839–848. doi:10.1088/1742-2132/12/5/839.

Mavko, G, Mukerji, T, 1998. Bounds on low-frequency seismic velocities in partially saturated rocks. Geophysics. doi:10.1190/1.1444402.

Mavko, G, Mukerji, T, Dvorkin, J, 2009. The Rock Physics Handbook: Tools for Seismic Analysis of Porous Media. doi:10.1017/CBO9780511626753.

Mindlin, R D, 1949. Compliance of elastic bodies in contact. J. Appl. Mech., ASME 16, 259–268.

Munir, K, Iqbal, M A, Farid, A, Shabih, S M, 2011. Mapping the productive sands of Lower Goru Formation by using seismic stratigraphy and rock physical studies in Sawan area, southern Pakistan: a case study. J. Pet. Explor. Prod. Technol.. doi:10.1007/s13202-011-0003-9.

Murphy, W, Reischer, A, Hsu, K, 1993. Modulus Decomposition of Compressional and Shear Velocities in Sand Bodies. doi:10.1190/1.1443408.

Nur, A, Mavko, G, Dvorkin, J, Galmudi, D, 1998. Critical Porosity: A Key to Relating Physical Properties to Porosity in Rocks. doi:10.1190/1.1437977.

Ødegaard, E, Avseth, P, 2004. Well log and seismic data analysis using rock physics templates. First Break 22, 37–43. doi:10.3997/1365-2397.2004017.

Qiang, Z, Yasin, Q, Golsanami, N, Du, Q, 2020. Prediction of reservoir quality from log-core and seismic inversion analysis with an artificial neural network: a case study from the sawan gas field, Pakistan. Energies 13, 486.

Raymer, L L, Hunt, E R, Gardner, J S, 1980. An improved sonic transit time-to-porosity transform. In: SPWLA 21st Annual Logging Symposium 1980.

Reuss, A, 1929. Berechnung der fließgrenze von mischkristallen auf grund der plastizitätsbedingung für einkristalle. ZAMM-Journal Appl. Math. Mech. für Angew. Math. und Mech. 9, 49–58.

Rider, M, 2002. The Geological Interpretation of Well Logs. Rider-French Consult. Ltd.

Vernik, L, 1997. Predicting porosity from acoustic velocities in siliciclastics: a new look. Geophysics 62, 118–128. doi:10.1190/1.1444111.

Voigt, W, 1910. Weiteres zu der Bernoullischen Methode der Bestimmung der optischen Konstanten von Metallen. doi:10.1002/andp.19103381410.

Walton, K, 1987. The effective elastic moduli of a random packing of spheres. J. Mech. Phys. Solid. 35, 213–226. doi:10.1016/0022-5096(87)90036-6.

Wang, Z, 2001. Fundamentals of seismic rock physics. Geophysics. doi:10.1190/1.1444931.

Wang, Z, Nur, A M, Batzle, M L, others, 1990. Acoustic velocities in petroleum oils. J. Petrol. Technol. 42, 192–200. doi:10.2118/18163-MS.

Widarsono, B, 2012. Choice of water saturation model in log analysis and its implication to water saturation estimates--a further investigation. Sci. Contrib. Oil Gas 35.

Yasin, Q, Du, Q, Ismail, A, Shaikh, A, 2019. A new integrated workflow for improving permeability estimation in a highly heterogeneous reservoir of Sawan Gas Field from well logs data. Geomech. Geophys. Geo-Energy Geo-Resources 5, 121–142. doi:10.1007/s40948-018-0101-y.

Yasin, Q, Du, Q, Yuan, G, Ismail, A, 2017. Application of Hydraulic Flow Unit in Pore Size Classification 3872–3876. doi:10.1190/segam2017-17494291.1.

Zahid, M, Durrani, A, Khan, M R, Ahmed, H, Naseem, N, Rehman, M A, 2016. Best Rock Physics Strategies in Reservoir Characterization : A Case Study from Lower Indus Basin of Pakistan Best Rock Physics Strategies in Reservoir Characterization : A Case Study from Lower Indus Basin of Pakistan.